Energy Storage Materials 41 (2021) 448–465

Contents lists available at ScienceDirect

Energy Storage Materials

journal homepage: www.elsevier.com/locate/ensm

Advanced strategies for the development of porous carbon as a Li host/current collector for lithium metal batteries

Rajesh Pathak[a,b], Ke Chen[a], Fan Wu[c], Anil U. Mane[b,*], Ratnakumar V. Bugga[d,*], Jeffrey W. Elam[b,e,*], Quinn Qiao[f,*], Yue Zhou[a,*]

[a] Department of Electrical Engineering and Computer Science, South Dakota State University, Brookings, SD, 57007, USA
[b] Applied Materials Division, Argonne National Laboratory, Lemont, IL, 60439, USA
[c] School of Science and Key Lab of Optoelectronic Materials and Devices, Huzhou University, Huzhou, Zhejiang, 313000, China
[d] Jet Propulsion Laboratory, California Institute of Technology, Pasadena, California, 91109, USA
[e] Advanced Materials for Energy-Water Systems Energy Frontier Research Center, Argonne National Laboratory, Lemont, IL, 60439, USA
[f] Mechanical and Aerospace Engineering, Syracuse University, Syracuse, NY-13244, USA

ARTICLE INFO

Keywords:
Lithium metal anode
Lithium-host/current collector
Porous carbon/Li composite
Solid-electrolyte-interphase
High-energy-density
Lithium metal batteries

ABSTRACT

Lithium metal is considered a promising anode material for high-energy-density rechargeable batteries because of its high specific theoretical capacity (3860 mAh g^{-1}), low mass density (0.534 g cm^{-3}), and low electrochemical redox potential (-3.04 V vs. the standard hydrogen electrode). However, the high reactivity of Li with the electrolyte leads to the formation of an unstable solid electrolyte interphase (SEI) and continuous side reactions. Also, the non-uniform lithium-ion flux and infinite volume expansion of Li metal cause the growth of Li dendrites. These pose significant safety challenges and cause rapid capacity fading of the lithium metal batteries (LiMBs). To resolve these issues, a low-cost, easily processed, lightweight, high-performance carbon-based porous matrix is considered promising to host Li metal deposition. The three-dimensional (3D) porous nano/microstructured carbon provides sufficient space for Li accommodation during Li plating, buffers the volume changes during Li plating/stripping, and lowers the effective current density contributing to dendrite-free Li deposition. Besides, the outstanding electrochemical and mechanical stability, flexibility and the high electronic conductivity enable the nano/microstructured carbon to serve as both Li host and current collector. The development of 3D carbon/Li composite by mechanical roll-press techniques not only eliminates the complex and risky procedure of making carbon/Li composite based on Li plating or molten Li infusion but also stabilizes the capacity at higher Li plating/stripping rates. Recently, there is an advancement in the lithiophilic decorations of 3D structure to introduce sufficient nucleation sites and the development of artificial SEI on top of the 3D matrix to suppress Li dendrite formation. Such 3D structural modifications create a uniform electric field, lower the Li nucleation overpotential, provide strong mechanical and chemical stability, and stabilize the interface thereby inhibiting the degradation of lithium and the electrolyte. In this review, we summarize the research progress on porous carbon/Li composites in terms of materials type, structure, fabrication technique, their electrochemical battery performance, and identify the critical challenges that need to be addressed for high-energy-density practical LiMBs.

1. Introduction

State-of-the-art lithium (Li)-ion batteries (LIBs) with graphite as an anode are reaching their practical specific energy density limit [1,2]. It is challenging to meet the demands for current energy storage and power requirements mainly in electric vehicles, microgrids, and portable electronics with the conventional Li-ion systems [3–5]. The lithium metal anode (LiMA) is considered as a promising candidate to replace the graphite anode because of its high specific theoretical capacity (3860 mAh g^{-1}), low mass density (0.534 g cm^{-3}), and low electrochemical redox potential (-3.04 Vs standard hydrogen electrode) [6–8]. The LiMA is expected to provide specific energy of 500 Wh kg^{-1} or higher at the cell level when coupled with high capacity/voltage cathodes such as high Ni- $LiNi_xMn_yCo_zO_2$ (NMC), 5V-spinel ($LiMnNiO_4$, LMNO), or multi-valent conversion cathodes, e.g., metal fluorides, sulfur, and environmentally-accessible oxygen [9,10]. However, major challenges are associated with the high-volume expansion, highly reactive nature, and aggressive electrochemical nature of LiMA in practical cells. The for-

* Corresponding authors.
E-mail addresses: amane@anl.gov (A.U. Mane), ratnakumar.v.bugga@jpl.nasa.gov (R.V. Bugga), jelam@anl.gov (J.W. Elam), quqiao@syr.edu (Q. Qiao), yue.zhou@sdstate.edu (Y. Zhou).

https://doi.org/10.1016/j.ensm.2021.06.015
Received 23 March 2021; Received in revised form 5 June 2021; Accepted 10 June 2021
Available online 17 June 2021

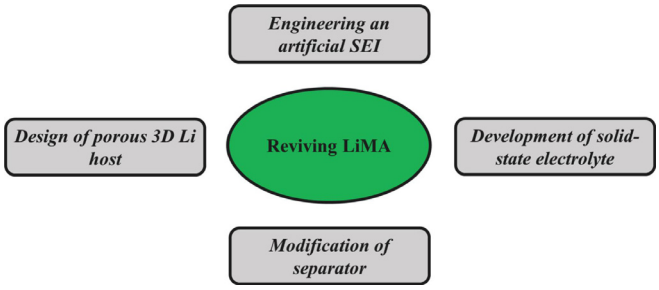

Fig. 1. Schematic of the different strategies for reviving Li metal anode.

mation of Li dendrites and unstable solid electrolyte interphase (SEI) not only challenge the safety but also limit the cycling performance of batteries that incorporate the LiMA. The *in-situ*-derived SEI lacks adequate electrochemical stability. The fragile and unstable SEI breaks down leading to continuous consumption of Li and electrolyte during repeated SEI formation or Li passivation.

Numerous efforts have been devoted to realizing stable LiMA, including the application of solid-state electrolytes [11–19], *in-situ/ex-situ* protective layers on top of LiMA [20–29], modification of the separator [30–40], and advanced three dimensional (3D) Li hosts [41–48] as shown in the schematic Fig. 1. Other approaches such as insertion of an interlayer [49–52] and implementation of compressive force during Li deposition [53,54] are also widely adopted for protecting the LiMA from dendrite formation or propagation. The use of an optimized electrolyte with suitable electrolyte additives, co-solvents, and salts can homogenize the Li-ion flux. Despite increased control over the Li dendrite growth and improved battery performance, the *in-situ* developed SEI even with additives, co-solvents, or highly concentrated Li salts has poor cohesion with the metal surface and lacks controllability on the dimension/distribution of SEI components. Consequently, the *in-situ*-derived SEI usually cracks due to the volumetric expansion of Li during Li deposition. The excess amount of Li and electrolyte consumed in the initial cycles for SEI formation lead to rapid capacity fading. In the case of the solid electrolyte, a great deal of research has focused on high modulus solid-state electrolytes which can effectively suppress Li dendrite growth. The physical blocking of Li dendrite growth, however, does not alter or improve the fundamental electrochemical properties during Li plating/stripping cycles. Besides, the interface incompatibilities and the low ionic conductivity of most solid electrolytes lead to high interfacial impedance and low power output. Moreover, cells manufactured using true polymer electrolytes and ceramic solid electrolytes typically must be operated at elevated temperatures at the expense of mechanical stability. The development of *ex-situ* artificial SEIs, either by physical deposition or chemical reaction deposition, is another strategy to successfully utilize the LiMA [6,7,55]. Despite the noteworthy successes, scientists are still facing challenges to engineer highly flexible, conductive, and mechanically/chemically stable SEIs. The strong anchorage binding energy of the SEI with Li metal can also inhibit delamination of the SEI layer from the bulk Li electrode.

Recently, an advanced 3D Li host has attracted great attention in reviving the LiMA, because the 3D Li host can provide sufficient surface area to accommodate the high-volume expansion and regulate the Li plating and stripping during charge-discharge cycles. Besides, the reduction in the effective local current density due to the high surface area of the 3D host material inhibits the growth of Li dendrites. Despite these attractive features, the practical applications of such 3D frameworks have been impeded by various limitations. This review will focus on the limitations and direction to address them as briefly pointed below.

(1) The utilization of excess or flooded electrolyte to compensate for the loss due to the high specific surface area of porous carbon. The flooded amount of electrolyte accounts for the major proportion of the total weight of the cell, compromising the volumetric or gravimetric energy density. Thus, it is required to prevent such excess consumption of electrolyte in the porous carbon Li host.
(2) The fundamental in-depth understanding of dendrite-free Li deposition limit based on porous carbon with various pore size, pore-volume, and pore depth, which requires the optimization of the porous structure.
(3) The lack of Li-ion affinity towards porous carbon due to the lithiophobicity, flexibility, poor electrical conductivity of porous carbon structure. Besides, and low mechanical/chemical stability could deteriorate the material and structural disintegrity, leading to low CE and quick capacity fading. The improved lithiophilicity, flexibility, and mechanical/chemical stability can pave the pathway to achieve enhanced electrochemical cycling performance.
(4) The complex synthesis and high material/ manufacturing cost by simple C/Li composite anode preparation technique with effective large-scale production could help to commercialization.

Based on these considerations, the design and development of practical and efficient 3D porous carbon as a dual Li host/current collector is highly needed. The lean carbon/Li composite anode provides higher anode-specific capacity vs. cathode. The dual feature of 3D carbon/Li composite to accommodate Li and act as a self-supporting current collector with an artificial SEI could synergistically improve the LiMA and provide a pathway for its use in practical high-energy-density lithium metal batteries (LiMBs).

This review paper focuses on advancing concepts in designing 3D porous carbon as Li hosts/current collectors while identifying critical challenges, possible solutions, and promising prospects. The high surface area, electronic conductivity, and lithiophilicity of 3D porous carbon toward the further advancement of LiMBs are discussed. The key focus should be on developing an innovative 3D design that facilitates homogeneous Li deposition with a stable interface during long-term cycling emphasizing the feasibility of such 3D porous carbon Li host/current collector for high energy density LiMBs. Finally, the perspective of the current challenges, future directions to develop the advanced 3D carbon/Li composite, understand state-of-art characterization tools, and modeling techniques to achieve the goal of high-energy-density, practical LiMBs are presented.

2. Pathways toward advanced 3D Li host

The current collector is one of the key components to regulate the initial Li nucleation and subsequent Li deposition in LiMBs. The conventional planar current collectors for the anode of LiMBs such as copper (Cu), Li, and nickel (Ni) are prone to inhomogeneous and dendritic Li deposition. The spatial inhomogeneous electric field on the planar current collector renders the inhomogeneous growth of lithium nuclei. The lithium nuclei create hotspots for the accumulation of charge leading to the rapid growth of Li dendrites. These needle-shaped sharp protrusions can pierce the separator causing an electrical short-circuit and even fire or explosion. Besides, the high surface area of the dendritic Li growth consumes excess electrolyte, which can lead to electrolyte dry-out and premature death of the cell.

The development of advanced nano/microstructured Li hosts has been adopted to investigate the lithium deposition mechanism during lithium plating/stripping cycles. The advanced nano/microstructured current Li hosts can reduce the current density and provide sufficient room for lithium deposition. The numerous protuberance tips on 3D frameworks serve as charge centers to obtain a uniform electric field and manipulate the lithium deposition sites. The protuberant tips have high electric field intensity and can serve as nucleation sites for Li deposition. If the protuberant tips are uniform on the porous Li host the electric field intensity will be informed, inducing uniform Li nucleation. For example, Wang et al. engineered vertically aligned microchannels in the Cu current collector/Li host which demonstrate a tip effect but sup-

presses the Li dendrite growth [56]. This strategy relies on the widely accepted diffusion model known as Sand's law [57]. This law indicates that the time at which the lithium dendrite starts growing, τ, follows a power as a function of the current density:

$$\tau = \pi D\, eC_o\left(\mu_a+\mu_c\right)^2/2J\mu_a \quad (1)$$

Where D is the ambipolar diffusion coefficient, e is the electronic charge, C_o is the initial Li concentration in the bulk electrolyte solution, μ_a and μ_c are the anionic and cationic mobilities and J is the practical effective current density at the electrode surface. The porous host reduces the effective current density for Li plating/stripping and provides enormous rooms to accommodate the deposited Li inside, maintaining dimensional stability.

Therefore, a higher surface area of the Li host at the electrolyte interface lowers the practical current density, J, and increases the Li dendrite onset time, τ, which consequently delays the nucleation of dendrites. Numerous efforts have been carried out in exploring the micro/nanostructured sized framework to reduce the effective current density during Li deposition. Although the small-sized porosity in the Li host increases the surface area, the insertion of Li inside the porous structure might be blocked. In contrast, the large porosity in the framework does not have any effect in confining the Li which could lead to Li detachment from the backbones and consequent electric contact loss and induces Li dendrite growth. Thus, the suitably optimized porosity of nano/microstructured porous Li host is crucial in confining the Li deposition and suppressing Li dendrite growth. Tuning the pore structure significantly influences the distribution of the electric field and eventually the Li-ion flux. Thus the pore size distribution greatly dictates the Li plating/stripping behavior. 3D porous framework for Li host has the diameter ranging from nanometer to tens of micrometer. Zhang et al. grouped different Li hosts based on their pore diameter size [186]. They are (1) small: pore diameter < 1 μm, (2) medium: pore diameter ranging from 1 μm to 10 μm and (3) large: pore diameter > 10 μm.

The smaller pore size Li host has a higher specific surface area which reduces the effective current density significantly compared to medium or large pore size Li host. Thus, according to Sand's law, uniform Li deposition and high rate capability can be expected. However, at the same time, the high surface increases the electrode/electrolyte contact area, consuming a tremendous amount of electrolyte during SEI formation. Besides, the high surface area of porous Li host will spread the Li deposition in the structure and a surplus amount of electrolyte comes in contact with the Li. This direct contact of Li and electrolyte render side reaction, consuming both lithium and electrolyte. This higher consumption of electrolyte results in the electrolyte dry-out and increases the impedance for Li-ion transport. Eventually, the undesired consumption of liquid electrolyte and lithium metal results in the premature death of the cell. In addition, the accumulated SEI or dead Li on the small porous structure could further block the pathway for Li-ion transport. As a result, the active surface area of porous carbon is reduced and cannot be fully utilized [64,186]. Lee et al. studied the Li plating/stripping mechanism in microporous carbon (MSP-20) with pore size < 2.0 nm and pore volume 1.0 $cm^3\ g^{-1}$, and mesoporous carbon (CMK-3) with pore size 3.4 nm and pore volume 1.3 $cm^3\ g^{-1}$. Although MSP-20 has a high surface area (2110 $m^2\ g^{-1}$), its CE started decreasing after 80 cycles and cells died around the 110th cycle. CMK-3 electrode with lower surface area (1120 $m^2\ g^{-1}$) delivered CE > 95% and remain almost steady up to the 200th cycle. CMK-3 electrode could easily regulate the Li-ion transport. Thus, it can be implied that Li plating/stripping does not only depend on τ but also the pore structure of the Li host.

Similarly, the large porous structure in carbon-based Li host yield high lithiation capacity, lowers the effective current density and accommodates a large amount of Li volume expansion. The high conductivity enables fast Li-ion transport, enabling superior high rate performance. For example, Zhang et al. employed the unstacked 3D hexagonal graphene drum as conductive nanostructured scaffolds with SSA of 1666 $m^2\ g^{-1}$, pore volume of 1.65 $cm^3\ g^{-1}$, and electrical conductivity of 435 S cm^{-1} [57]. Such large pore volume unstacked graphene facilitates a high theoretical Li cycling capacity of 4 mAh g^{-1}, reflecting the importance of large pore volume in nanostructure in LiMA. However, if the pore volume of the Li host is too big, instead of deposition, the Li metal can be easily detached from the backbone of the porous structure, resulting in electrical disconnection. For example, Guo et al. reported that a 3D porous Li host with a large pore volume of 0.58 $cm^3\ g^{-1}$ does not have any effect of space constraint leading to Li dendrite growth [73]. 3D Li host with large pore size of 170 μm and pore volume of 0.58 $cm^3\ g^{-1}$ create a large amount of inactive dead Li and demonstrate very poor CE ~ 40% at around 20th cycle of Li plating/stripping.

Pore depth also governs the morphology of the Li deposition as the electric field distribution can be varied by tuning the pore depth. While increasing the pore depth from 50 to 150 μm, the current density increases from 70.4 to 160.1 mA cm^{-2} according to the phase-field model [58]. The variation in the diameter of deposited Li due to variation in pore depth creates variation in the effective surface area and eventually the effective current density [56,58].

The porous structure of carbon is always challenging in making C/Li composites by any of the methods (electrodeposition, molten Li infusion, or mechanical roll press). During Li electroplating or molten Li infusion, lithium metal might be clogged inside the very small porous structure and in some cases, it might get electrical disconnection due to a very large porous structure. Similarly, while making C/Li composite by mechanical roll/press method, the process may result in inhomogeneous Li metal distribution or could accumulate on the surface of the carbon. The porous carbon modifications using lithiophilic materials can help to distribute the Li deposition uniformly, however, it is very tricky during the process of making C/Li composite with high uniformity, into the complex porous structure.

The high flexibility and mechanical stability of interconnected porous framework serve as Li storage reservoir, buffering the large Li volume expansion issue and inhibiting the loss of active material during electrochemical cycling performance. The high flexibility and mechanical stability in carbon-based Li hosts can retain its original shape/structure after repeated folding and unfolding test or coiling the carbon-based strip around the glass rod [58–62]. The outstanding flexibility and mechanical stability in terms of toughness or ductileness of porous carbon Li host help to buffer the huge internal stress and fluctuations during fast charge/discharge or repeated Li plating/stripping cycles, suppressing the Li dendrite growth and inhibiting the electrode disintegration or collapse [63]. The modulus of the porous carbon-based Li has a higher Young's modulus than the threshold of 6.0 GPa, sufficient to suppress the Li dendrite [136]. Carbon is chemically stable with the Li metal and with the liquid electrolyte, preventing side reactions. Besides carbon offers excellent electrochemical stability during long or high-rate charge/discharge. The high electrochemical stability of interconnected porous carbon contributes to the formation of stable SEI. The unchanged structure of the porous carbon framework during electrochemical cycling helps to maintain stable capacity. Thus, the high flexibility, mechanical stability of the porous carbon are of great importance in battery manufacturing, as pouch cell or cylindrical cell, configurations require high flexibility and mechanical strength during folding or rolling process and the chemical stability maintain the structural integrity and form robust SEI during the electrochemical cycling performances [137–140].

The uniform electronic conductivity within the porous carbon also helps to obtain uniform Li deposition. The high conductivity of the porous carbon is equally important to capture or withhold the deposited Li [59–62]. Liang et al. reported uniformly distributed silver nanowire (AgNW) on 3D graphene as the host for Li metal composite anode [63]. The intrinsic high electrical conductivity of AgNW facilitates the fast charge transport, guiding the high capacity of lithium at a high current density. The high graphitization in the porous carbon Li host increases the conductivity which leads to fast Li-ion transport [64–68].

The gradient of electrical conductivity in the porous Li host could lead to uneven Li deposition because the area with high electronic conductivity captures the Li-ions quickly than the area with poor electronic conductivity. The higher electrical conductivity material will produce more current flow than the poor electrical conductivity material, creating a difference in the electric field within the Li host. The structure with poor electrical conductivity has large electrical impedance and strong polarization. When compared with the poor conductive area, the higher electronic conductive area accumulates the Li deposits which act as a hotspot leading to lithium dendrite growth. Thus, the non-uniform Li-ion flux due to the gradient of electrical conductivity in the porous Li host could lead to Li dendrite growth. In contrast, the uniform Li deposition can be expected if we use two bilayers as SEI, for example, poor electronic conductive on top of the high electronic conductive layer. In such a case, the poor electronic conductive layer should allow sufficient Li-ion diffusion, allowing the deposition on the high electronic conductive bottom layer. Various conductive 3D porous Li hosts such as metals and carbon have been widely investigated. Other 3D porous non-conductive Li hosts such as h-BN [69,70], polyacrylonitrile, polyimide [71], poly-melamine-formaldehyde [72], and glass fibers [51] have also been studied in LiMBs.

Metals such as copper (Cu), nickel (Ni), Titanium (Ti), stainless steel, and Li have been widely reported to develop a three-dimensional (3D) nanostructured Li host. The metal-based Li host has excellent electronic conductivity which can easily capture Li-ions and reduce the chances of dead Li formation. Researchers have developed various nanostructures on the Cu-metal-based Li host such as porous Cu [73–77], copper nanowires (CuNW) [78,79], 3D pie-like structures [80], vertically aligned Cu [81], and Cu foams [73,82]. The other metal-based nano/microstructured Li host employed includes Ni foam [83] and Ti [84,85], stainless steel fibers [49], and porous lithium metal foam [86]. In general, the electric field between the electrodes inside the battery is predominantly scattered in a vertical configuration, vertically favoring the Li dendrite growth. This vertical growth of sharp needle-shaped dendrites can pierce the separator, causing an internal short-circuit. To overcome this, scientists have been working continuously to design a series of porous frameworks which create a more uniform electric field. Wang et al. designed vertically aligned microchannels in Cu to accommodate the maximum amount of Li inside the microchannels [81]. As the pore diameter, pore depth, and pore spacing determine the average particle size, shape, or morphology of the deposited Li, optimization is required to deposit most of the lithium inside the microchannel. The optimized pore radius of 5 μm, pore depth of 50 μm and pore spacing of 12 μm (Cu-5–50–12) showed the least overpotential of ~144 mV at a current density of 1 mA cm^{-2} compared to the other conditions as shown in Fig. 2a. The planar Cu showed a non-uniform Li deposition, however, the porous Cu-5–50–12 showed uniform, spherical shaped Li deposition into the vertically aligned microchannels (Fig. 2b,c). Zou et. al designed a Li host which exhibited a laterally oriented electric field which consequently facilitated Li deposition in the lateral pattern [87]. Fig. 2d-f shows the stripping/plating and subsequent stripping of the Li with dendrite-free Li deposition and complete stripping of the Li.

To further govern the initial Li nucleation and subsequent voltage hysteresis, Zhang et al. developed lithiophilic, nitrogen-doped graphene-modified 3D Cu (3DCu@NG) where the scattered distribution of electrons shows a strong Li-ion affinity [88]. Fig. 2g shows a schematic of Li deposition in 3DCu@NG and Figs. 2h-l show the Li morphological evolution on 3DCu@NG at 0.5 mA cm^{-2} at different amounts of Li deposition. As the Li plating areal capacity increases, the pore size decreases owing to the strong interaction between the N-doped graphene and Li. Fig. 2m shows the complete retaining of the initial morphology of 3DCu@NG with SEI. Fig. 2n shows the schematic of the Li deposition in 3D Cu. In contrast, 3D Cu shows uneven and lumpy Li deposition (Figs. 2o-t) owing to the weak interaction between 3D Cu and Li-ion. Besides, after complete Li stripping, the 3D Cu shows broken SEI with Li residues indicating high irreversibility (Fig. 2u). The use of a lithiophilic coating or decoration on the metal-based porous Li host has now been widely adopted for smooth Li deposition and reducing the voltage overpotential [89–97]. The design of conductivity and lithiophilicity gradient approach reported by Pu et al. showed excellent electrochemical performance up to 40 mAh cm^{-2} at a high current density up to 30 mA cm^{-2} and low temperature down to -15 °C [98]. The 3D scaffold framework was electrically passivated on the top region using an Al_2O_3 coating and chemically activated on the bottom region using an Au coating. Recently, the design of Li/3D metal porous structure composites by molten Li infusion or by mechanical pressing has been considered as an advanced technique to eliminate the electroplating, complex disassembling, and electrode cleaning steps [83,99–102]. However, the metal-based Li host has a high cost, high density, and is electrochemically unstable to moisture and oxygen. Besides, the complex engineering process of metal-based nanostructured materials limits their further practical application. Thus, more attempts should be done on reducing the cost and facilitating the processability before the commercialization of such a metal-based Li host. To circumvent these shortcomings, the 3D porous carbon structures grown on the metal-based current collector are designed [103]. 3D carbon-based materials can be easily processed and possess better flexibility to buffer the volume change of Li during plating/stripping cycles. Self-supporting, 3D porous carbon materials are considered promising next-generation Li hosts owing to their low cost, natural abundance, and low density. In this review, the advancement of the fundamental challenges associated with 3D porous carbon such as low conductivity, unstable SEI, and low lithiophilicity will be discussed in detail.

The high mass density which leads to low energy density, inflexibility, complex and expensive processing cost of metal-based Li host challenges its applications in LiMBs. To integrate the advantage of both metal and carbon, the modification of the 3D metal current collector with carbon is a good choice. We reported the copper-clad carbon framework (CuCF), where the carbon framework provides flexibility in the backbone and the ultrathin/rough surface layer of Cu provides high electronic conductivity and lithiophilicity. Figs. 3a-c show the voltage profile of Li plating at various capacities up to a total Li deposition of 4 mAh cm^{-2}. The CuCF (obtained after electroplating Cu on CF for 6 mins) shows the lowest nucleation overpotential of 29.0 mV compared to 47.1 mV and 150 mV for CF and planar Cu, respectively, indicating well-distributed nucleation sites and the highest lithiophilicity of CuCF. Figs. 3d-e show the corresponding SEM images of planar Cu, CF, and CuCF after plating 4 mAh cm^{-2} amount of Li on them. CuCF (Fig. 3d) shows dendrite-free and smooth Li deposition compared to the dendritic, whisker Li deposition on planar Cu (Fig. 3d) and CF (Fig. 3e). The long fibrous dendritic Li deposition could break during the Li stripping cycle, forming inactive dead Li. Fig. 3g shows a cross-sectional SEM image of a single fiber in the CuCF electrode with ~200 nm Cu layer after electroplating of Cu on CF. The CuCF electrode shows a higher CE of 99.5 % even after 300 cycles (~1200 h) at 0.5 mA cm^{-2} compared to planar Cu and CF due to the synergy of electronic conductivity, lithophilicity induced by rough Cu surface, and the flexible backbone support CF as shown in Fig. 3h.

3. Advanced strategies for development of porous carbon Li host

3.1. Porous carbon coated on metal-based current collector

Among various 3D porous Li hosts, carbon has been regarded as an ideal Li host due to its light-weight, flexibility, high mechanical and chemical stability, high electronic conductivity, low cost, and natural abundance. To protect the LiMA from side reactions with the liquid electrolyte and to accommodate the Li deposition, various porous carbon matrices such as carbon nanotubes (CNT), carbon nanofibers (CNF) [104,105], graphitized carbon fiber/foams [68,106], hollow carbon nanospheres [103,107], multilayer-graphene [108–113], graphene-CNT hybrids [114], reduced graphene oxide (rGO) [115], and metal-

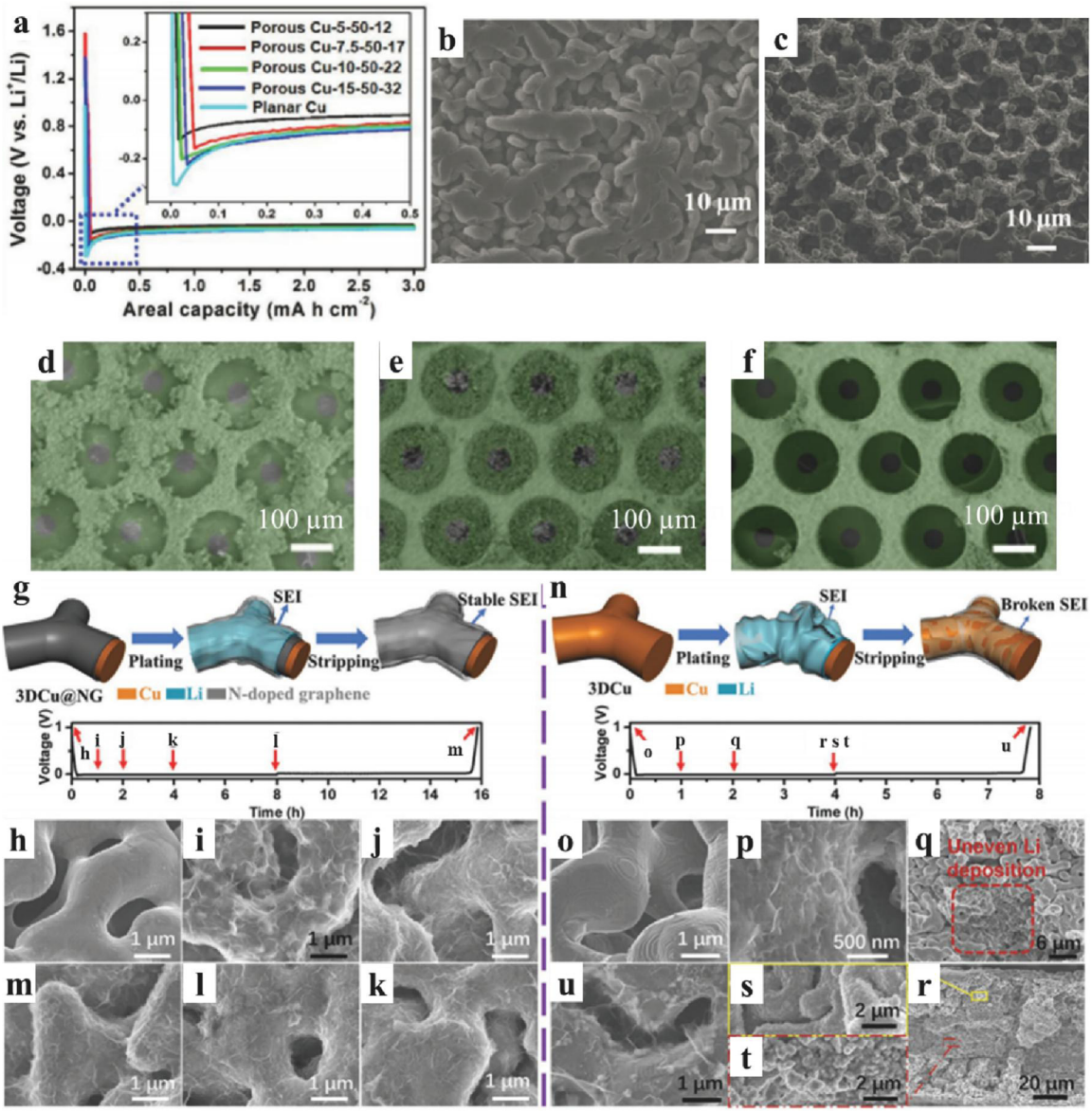

Fig. 2. Metal-based porous framework for dendrite-free Li deposition. a Voltage-areal capacity profile with different Cu current collectors. Reproduced with permission from Ref. [81], John Wiley and Sons. **b,c** SEM images of Li deposition in planar Cu and Cu-5–50–12 current collector. **d-f** SEM images after stripping 1 mAh cm^{-2} from 2 mAh cm^{-2} deposited E-Cu followed by subsequent 1 mAh cm^{-2} Li deposition and all Li stripping. Reproduced with permission from Ref. [87], Springer Nature. Schematic representation of Li plating/stripping on **g** 3DCu@NG and **n** 3D Cu. SEM morphology for various amounts of Li deposition at 0.5 mA cm^{-2} on **h-m** 3DCu@NG and **o-u** 3DCu.Reproduced with permission from Ref. [88], John Wiley and Sons.

organic frameworks [116] have been deposited on metal current collectors such as Cu, Ni or Li. Besides coating on the current collector, separate interlayers have been employed to stabilize the SEI and revive the LiMA. The electrical conductivity between the carbon and the bulk metal current collector underneath allows the bottom-to-top deposition of Li. The growth of Li dendrites underneath the porous carbon after several cycles of Li plating is further suppressed by the high Young's modulus of the carbon. Moreover, the highly porous and flexible carbon accommodates the volumetric Li expansion without any mechanical destruction. In comparison, a compact coating of carbon thin film on the current collector may crack upon cycling due to the lower flexibility and insufficient space for Li accommodation and the protrusion of Li dendrites.

Zheng et al. fabricated hollow carbon nanospheres by a template synthesis method (Fig. 4a-c) to modify a Cu/Li current collector [103]. Fig. 4d shows an SEM image of the carbon-coated polystyrene nanospheres and the inset shows a digital photo of the as-fabricated hollow carbon nanospheres after removing the polystyrene template. The photograph shows the bending ability of the hollow carbon nanospheres. At the beginning of the Li deposition, Li nucleates on the Cu substrate within the hollow carbon nanospheres. As Li deposition continues, granular Li elevates the hollow carbon nanospheres, indicating the high flexibility of carbon and deposition of Li underneath the carbon. Cheng et al. reported *in-situ* formed SEI-coated on nanostructured graphene framework (GF) denoted as (SCG) which provides both electron and ion channels to improve the charge transport properties and recycle the dead Li [117]. The GF exhibited a pore volume of 1.6 mL g^{-1}, an average pore size of 10 nm, and ionic conductivity of $7.81^{*}10^{-2}$ mS cm^{-1}. Fig. 4e shows the schematic and Fig. 4f shows an SEM image of Li deposition/dissolution in SCG. The polysulfide-containing electrolyte stimulates the thin (~10 nm), smooth, robust, and stable SEI on the surface of the porous and interconnected graphene framework.

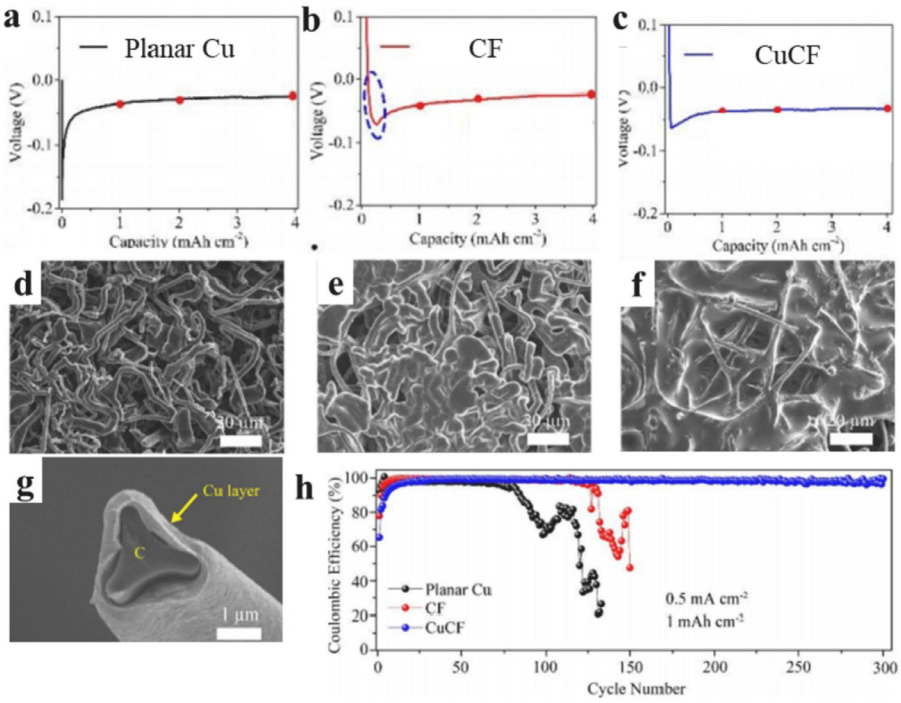

Fig. 3. **a-c** voltage profile of Li plating at 0.5 mA cm^{-2} to achieve a capacity of 4 mAh cm^{-2} on planar Cu, CF and CuCF electrode. and corresponding SEM image during 4 mAh cm^{-2} Li plating. **d-f** corresponding SEM image of the planar Cu, CF and CuCF electrode after Li deposition of 4 mAh cm^{-2} capacity. **g** cross-sectional SEM image of CuCF. **h** CE test of planar Cu, CF and CuCF electrode at a current dfensity of 0.5 mA cm^{-2} to achieve a capacity of 1 mAh cm^{-2}. Reproduced with permission from Ref. [82], Royal Society of Chemistry.

Such thin-film SEI lowered the Li-ion diffusion resistance. Besides, the GF has a high density of structural defects which act as Li nucleation sites, and the GF nanopores provide sufficient interspace for Li deposition. The lower electrical conductivity of the nanostructured Li host results in a large electrical impedance and large voltage overpotential at a higher charging/discharging current density rate. Zhang et al. designed unstacked GF with a hexagonal 3D drum-like structure with two layers exhibiting a large specific surface area of 1666 m^2 g^{-1}, a pore volume of 1.65 cm^3 $g^{-1,}$ and electrical conductivity of 435 S cm^{-1} [104]. Figs. 4g,h show Li deposition behavior on the graphene flake. The homogeneously deposited Li on the graphene drum form a sandwich-like, core-shell structure, which consists of graphene as the core, the lithium as the outer shell, and the SEI as the outermost shell. The dual salt (LiTFSI-LiFSI) electrolyte and nanostructured GF retain a highly flexible and robust SEI, which allows Li deposition underneath the SEI (yellow) on the graphene flakes thereby maintaining stable cycling of the LiMBs. Graphite-based carbon anode materials have already been commercialized in LIBs owing to their appropriate layered structure, high electronic/ionic conductivity, and storage ability by intercalation. Ye et al. have effectively exploited the benefit of graphite materials as Li hosts for stable Li plating/stripping cycles [118]. Each carbon (C) atom on the planar graphite has an unpaired and delocalized π electron which induces weak interaction with dissociated Li-ion of the electrolyte (Fig. 4i). In contrast, each C-atom on the curved graphite has a partially localized π electron (Fig. 4j), enhancing the binding affinity towards Li-ions. The insertion of Li into curved graphite leads to the formation of the C/Li composite, which further enhances the electronegativity of the C-atom on the curved graphite (Fig. 4k). The numerous layers of curved graphite facilitate a uniform Li-ion flux, which results in enhanced Li wettability. This results in uniform Li plating and stabilized mass/charge transfer across the interphase. Fig. 4l shows that during initial plating/stripping cycles, the pre-plated Li in the nanogap of the graphene layer can reversibly be stripped back, where most of the Li-ions remain in their intercalation state. During extensive plating/stripping cycling, pre-plated Li in the nanogap of the graphene layer progressively dissolves in the electrolyte leading to a reversible deintercalation of the Li-ions to compensate for any Li loss. As a result, a hybrid intercalation/nano-plating storage mechanism enables long-term stable cycling performance. In addition to the 3D porous carbon materials, the excellent electrical conductivity, lithophilicity, and open nanoscale vertical 3D structure in carbon can significantly improve the charge transport, govern the initial Li nucleation, provide sufficient room for Li deposition, and reduce the effective current density. Chen et al. designed a vertically aligned carbon nanofiber (VACNF) array with excellent conductivity and graphitic edge sites with a high density of oxygen-and nitrogen-containing functional group [119]. Figs. 4m,n show SEM images of pristine VACNF and dendrite-free 2mAh cm^{-2} Li deposited on the VACNF. The insignificant change in the thickness of VACNF after 2mAh cm^{-2} Li deposition indicates the effective suppression in Li volume expansion (inset of Fig. 4n). Pei et al. also designed lithiophilic 3D current collectors by using N-doped porous carbon nanosheets to modify metal-based Cu/Ni foams to create a yolk-shell structure [120]. Such a metal-modified current collector exhibit significantly improved capacity retention of 78.1% after 1400 cycles.

3.2. Porous carbon as interlayer

The uneven surface of the current collector creates large protuberances which induce a non-uniform electric field distribution. This results in the adsorption of Li-ions on the tip of protuberances called the “tip effect”. If there is a single tip or nonuniform tip, they can lead to the accumulation of Li deposition which acts as a hot spot for Li dendrite growth [51,121–123]. The accumulation of Li-ions at the tip creates a charge center that gradually leads to the formation of Li dendrites. The use of an interlayer between the current collectors and the separator helps to disperse the Li-ion flux. The poor electronic conductivity of the interlayer does not allow Li deposition on top of the interlayer rather, the Li-ion plating is diffused between the interlayer and current collector. However, the electronically conductive interlayer enables fast electron transport which induces fast Li plating. Other additional features such as lithiophilic functional groups and electronic conductivity govern initial Li nucleation for smooth Li deposition even at higher current densities. The ideal interlayer possesses a high electrolyte affinity, strong lithiophilicity, high Li-ion conductivity, and poor electronic conductivity. Recently, the mixed Li-ion and electronic conductive interlayers have also been widely adopted in LiMBs [124,125]. The uniform dis-

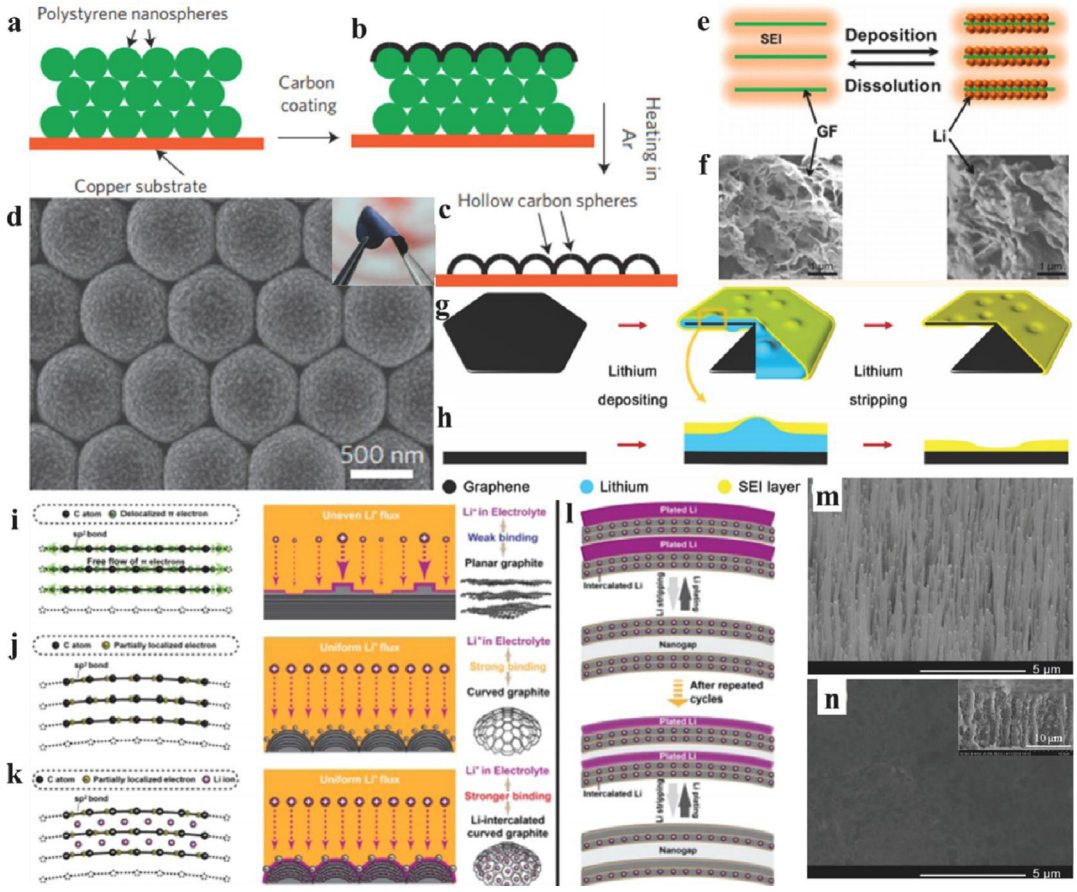

Fig. 4. Fabrication of porous structured carbon on the current collector. a-c Synthesis process of hollow carbon nanospheres on the Cu electrode. **d** SEM images of the carbon-coated polystyrene nanoparticle and the inset show the flexible as-fabricated hollow carbon nanospheres. Reproduced with permission from Ref. [103], Springer Nature. **e, f** Schematic and the corresponding SEM images of Li deposition/dissolution in GF. Reproduced with permission from Ref. [117], American Chemical Society. **g,h** Schematic illustration of Li plating/stripping on single graphene flake. Reproduced with permission from Ref. [104], John Wiley and Sons. **i-k** Mechanism of Li plating/stripping on planar graphite sheet, curved graphite sheet, and Lithiated curved graphite sheet, respectively. **l** backup source of Li in Li intercalated Carbon (C/Li) to compensate for the capacity loss. Reproduced with permission from Ref. [118], American Chemical Society. **m,n** Perspective SEM images of VACNF and 2 mAh cm^{-2} plated VACNF. The inset shows the cross-section of mAh cm^{-2} plated VACNF. Reproduced with permission from Ref. [119], John Wiley and Sons.

tribution of local electric-field on the interlayer, porous structure which provides the space for Li deposition and buffer the Li expansion contribute to the dendrite-free Li deposition, enabling improved battery performance. The use of various interlayers such as carbon paper on LiMA [126], glass fiber modified Cu [51], and polymer nanofiber modified Cu [127] have shown improved battery performance. Zhao et al. has reported dendrite-free Li deposition and almost 10 fold longer plating/stripping cycles with the use of carbon paper (CP) as an interlayer on top of the LiMA [126]. The strong mechanical stability and flexibility of CP contributed to stable electrochemical performance. Figs. 5a,b shows SEM images of the Li electrode with CP as interlayer after 3 mAh cm^{-2} of Li deposition. The uniform Li-ion flux and of the porosity of the CP allow smooth Li deposition. The CNF interlayer on both sides of the separator was demonstrated to control the tip effect for stabilizing the LiMA [128]. Fig. 5c shows a schematic of the uniform redistribution of electrons and Li-ions along with the CNF skeleton. Eventually, the uniform Li-ion flux renders smooth and dendrite-free Li deposition on the current collector. Xu et al. designed a multifunctional covalent organic framework (COF) as a Li protective interlayer [129]. The lithiophilic COF can immobilize anions and uniformly disperse Li-ions resulting in a uniform Li-ion flux (Fig. 5d) and yielding a dense and smooth Li deposition. The interlayer with high surface area, porous structure, and embedded with a polar functional group reduces the migration of soluble polysulfide intermediates, protecting the LiMA [130–135]. Kong et al. stabilized the LiMA and improved Li-S battery performance using porous carbon paper as the interlayer [134]. This interlayer prevents the shuttling of soluble polysulfides from cathode to anode and protects the LiMA from degradation. As a result, a smooth and dense Li deposition was obtained after 100 cycles (Fig. 5e). In contrast, a Li-S battery without interlayer is prone to the shuttling effect of lithium polysulfides leading to pulverization and cracks in the LiMA resulting in dendritic Li deposition (Fig. 5f). Interlayers other than carbon, such as glass fiber on Cu current collector [51] and 2D $Ti_3C_2T_x$ MXene on Li [127], have been reported to guide the Li deposition. Cheng et al. modified the Cu current collector with 3D glass fiber cloth (10 μm) with a sufficient number of polar functional groups such as Si-O, O-H, and O-B [51]. The presence of polar functional groups on glass fiber offset the electrostatic interactions between the Li-ion and protuberances on the current collector preventing the accumulation of Li-ions. The strong interaction between the Li-ions and the glass fiber induces a uniform Li-ion flux. Moreover, the non-conductive glass fiber allows the deposition of Li underneath the glass fiber and suppresses Li dendrite growth.

3.3. Lithiophilic 3D carbon matrix

The non-polar carbonaceous materials have a poor affinity towards Li. Thus, they cannot promote uniform initial Li nucleation and cannot infuse Li quickly into the inner porous structure. The introduction of

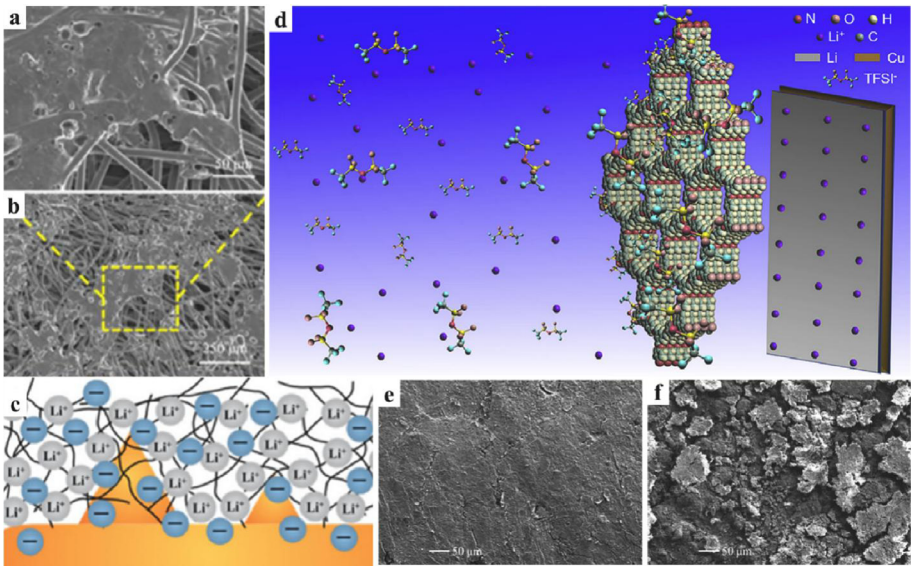

Fig. 5. Interlayers on the top current collector. **a** High-resolution SEM image corresponding to figure b. **b** Li deposition SEM topography of CP protected Li electrode. Reproduced with permission from Ref. [126], Elsevier. **c** Schematic of the anion-cation charge distribution using CNF on top of Cu current collector. Reproduced with permission from Ref. [128], Elsevier. **d** Schematic of the lithiophilic COF interlayer for immobilization and dispersion of anion-cation charges. Reproduced with permission from Ref. [129], Elsevier. **e,f** SEM images of Li electrode with and without porous CP interlayer. Reproduced with permission from Ref. [134], American Chemical Society.

polar species within the porous carbon material is essential for inducing uniform Li nucleation sites. The polar species such as (1) metal oxides, metal-organic frameworks, metal carbides, metal phosphides; (2) heteroatom dopants such as nitrogen (N), boron (B), oxygen (O), phosphorous (P); (3) metals with a high Li solubility such as gold (Au), silver (Ag) and silicon (Si); and (4) functional groups such as C=N, C-N, C=O, O-H, [127] C=O, N-H, [136] and -NH [137] can preferentially induce the nucleation of lithium. The higher Li cohesive energy of lithiophilic materials allows the Li-ion to interact strongly. Yan et al. studied the lithium nucleation overpotential on various substrates including Au, Ag, Zn, Mg, Al, Pt, Si, Sn, C, Cu, and Ni [138]. Among this representative list, some elements such as Cu and Ni do not react with Li at room temperature, showing higher overpotential. Elements such as Au, Ag, Zn, and Mg form an alloy with Li showing zero overpotentials. Although C, Sn, and Si form an alloy with Li, an overpotential is still observed. The voltage-capacity profile was studied to understand the Li nucleation overpotential and voltage overpotential. The Li nucleation overpotential is defined as the difference between the highest plating voltage (bottom of the voltage dip) and the stable voltage plateau. The overpotential is the voltage required to compensate for the heterogeneous nucleation barrier accompanied due to the thermodynamic mismatch between Li and the substrate. The Au, Ag, Zn, and Mg demonstrated zero overpotential owing to their highest solubility in Li as shown in Fig. 6a. The Ag and Mg also have a high solubility but showed a flatter sloping voltage profile before the onset of the Li deposition indicating the dissolution of these metals in Li. The Al and Pt showed Li nucleation overpotentials of 5 mV and 8 mV, respectively, indicating that they have lower solubility in Li. Fig. 6b shows the solubility test for Cu, Ni, Si, Sn, and C in Li. As they do not have solubility, both Cu & Ni which do not form alloy showed a high overpotential of around 30 mV, and Si, Sn, and C showed nucleation overpotentials of 13, 16, and 14 mV, respectively. Liang et al. coated the lithiophilic Si on porous carbon by chemical vapor deposition (CVD) [139]. The lithiophobic porous carbon due to the lack of bonding between the molten Li and carbon showed a droplet of molten Li on the carbon framework (Fig. 6c). In contrast, the Si-modified carbon framework formed a binary alloy phase-lithium silicide due to the interaction between the molten Li and the Si coating. This allowed the molten Li to wet the total surface of the porous framework (Fig. 6d).

Nitrogen (N) containing functional groups endow N-doped porous carbon with a lithiophilic surface that exhibits a dendrite-free morphology during Li plating/stripping cycles, enabling a high CE [140–143]. The high-resolution C 1 s spectrum from X-ray photoelectron spectroscopy (XPS) presents peaks at 285.9 and 287.2 eV, which can be assigned to C=N and C-N bonds, respectively [141]. The high-resolution N 1 s spectrum as shown in Fig. 6e presents peaks at ~ 398, ~ 400.1, and ~ 401 eV which can be assigned to pyridine, pyrrolic and quaternary nitrogen, respectively [144,145]. The pyrrolic nitrogen and pyridinic nitrogen have larger Li binding energies (BE) of -4.46 and -4.26 eV compared to graphene (-3.64 eV) and Cu (-2.57 eV) [146]. The pyrrolic nitrogen group contains one extra electron and the pyridinic nitrogen group contains lone-pair electrons. The N-containing Lewis base site strongly adsorbs Lewis acidic Li-ions. In contrast, quaternary Nitrogen which has saturated electron orbitals cannot provide extra electrons to adsorb Li-ions, resulting in a lower BE. Chen et al. studied three key factors, electronegativity, local dipole, and charge transfer, to understand the origin of lithiophilicity of heteroatom doped porous carbon materials [147]. Based on these key factors, among single boron (B), N, and oxygen (O) doping, O-doped showed the best lithiophilicity, and among O-B/sulfur (S)/phosphorous (P) co-doped heteroatoms, O/B co-doping was predicted to deliver excellent lithiophilicity. This study provides a rational strategy to develop the single or co-doping of lithiophilic heteroatoms into the porous carbon framework for LiMBs. The use of various lithiophilic materials on nano/mirostructured porous carbon is summarized in Table 1.

Liu et al. reported the coordination of Co atom and N doping in the carbon matrix to tailor the local electronic structure, promoting the Li nucleation process [177]. Although sufficient N-doping could significantly improve the lithiophilicity of the carbon matrix, on the other side, it can dismantle the structural integrity, decreasing the electronic conductivity. The N heteroatoms in N-doped carbon initiate coordination with Co atoms forming Co-N_x-C. The higher electronegativity of CoN_x center in CoNC than N-site in N-doped carbon provides stronger Li-ions affinity. Besides, heteroatoms, diverse metal oxides such as ZnO, CuO, SnO_2, SiO_2, and NiO with fairly high lithiophilicity have been proposed to introduce uniform Li nucleation sites and stabilizing the SEI [178]. However, the low electrical conductivity of most oxides is problematic in promoting a uniform Li-ion flux, especially at higher current densities. Metal oxide can also undergo irreversible conversion reactions which form insulating Li_2O and result in low CE. Moreover, alloying reactions are typically accompanied by a large volume expansion. Thus, lithiophilic metal nitrides with higher electrical conductivity and electrochemical stability are considered more promising than metal oxides for delocalizing the Li plating/stripping current rates. The capacitive charge storage across the grain boundaries of conductive lithiophilic metal nitride also retards dendrite growth [156].

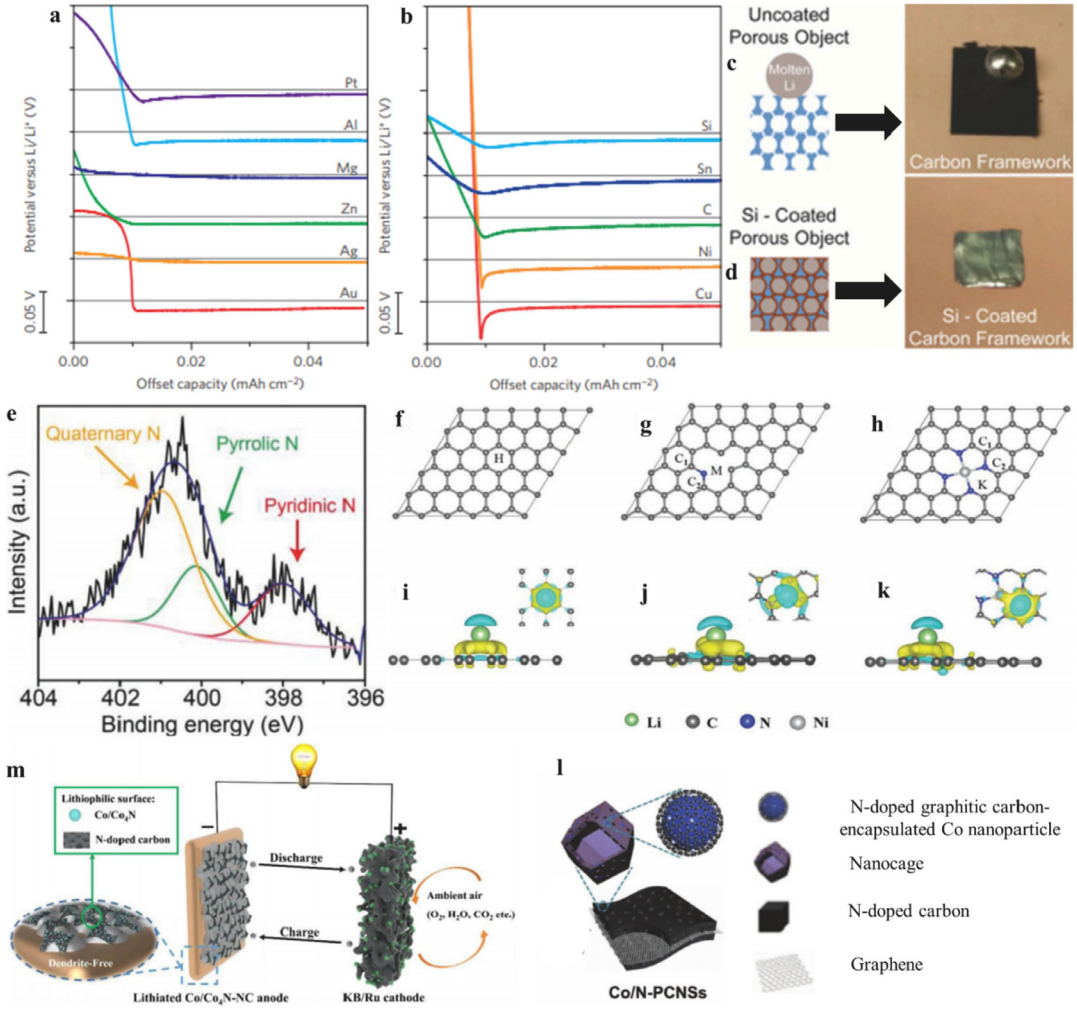

Fig. 6. **a,b** Voltage profile of various materials with some solubility and negligible solubility, respectively. Reproduced with permission from Ref. [138], Springer Nature. **c,d** Li wettability of porous carbon without and with lithiophilic Si coating. Reproduced with permission from Ref. [139], Proceedings of the National Academy of Sciences. **e** High-resolution N 1 s XPS spectra of N-doped graphitic carbon foams. Reproduced with permission from Ref. [144], John Wiley and Sons. **f-h** Top view, and **i-k** side view of PG, NG, and SANi-NG, respectively, showing the Li adsorption site on their structure. H, M, and K indicate the most stable Li adsorption sites. C_1 and C_2 denote the C-atoms for N-atom bonding. Reproduced with permission from Ref. [145], John Wiley and Sons. **l** Schematic of cobalt-embedded N-doped porous carbon nanosheets (Co/N-PCNSs). Reproduced with permission from Ref. [180], John Wiley and Sons. **m** Schematic illustration of Li-air battery with lithiated Co/Co_4N-N-doped carbon nanocubes as an anode. Reproduced with permission from Ref. [157], Royal Society of Chemistry.

Table 1
Lithiophilic materials used in the different porous structures of carbon.

Lithiophilic material	Example	Carbon-based Li host	Ref.
Metal oxides	ZnO	3D porous carbon/CNT/graphene nested carbon fiber cloth/carbonized MOF	[148–152]
	SiO_2	CNT, carbon paper	[153,154]
	MnO_2,CO_3O_4,SnO_2	Graphene foams	[155]
Metal nitrides	TiN	CNF	[156]
	Co_4N+Co+N	Hollow carbon nanocubes	[157]
Metal carbides	LiC_6, TiC	Carbon fibers, carbon core/shell arrays	[158–160]
Metal-organic framework	Co_3O_4-N, Zn	Porous carbon nanoflake, carbonized porous MOF	[161,162]
Heteroatoms	Nitrogen-N	Carbon rod arrays, graphitic carbon foams, 3D nanoporous graphene	[144,163,164]
	Oxygen-O	Crumpled graphene balls, CNF	[165,166]
	N+O	CP, carbon cloth, carbon granules	[167,168]
	N+Phosphorous-P	Porous carbon	[169]
	Gold-Au	pillared rGO, carbon fiber	[170,171]
	Ag	CNF, carbon fiber framework	[172,173]
	Silicon-Si	Porous carbon	[139]
	N+Fe	Carbon matrix	[174]
	N+Fe+Ni	CNT	[175]
	C=O, N-H	Graphene oxide	[136]
	-NH	Mesoporous CNF	[137]
	-COOH, -NH_2, C-N, C-O, C=O, N-C-O	multi wall-CNT	[176]

The stability of the coordination structure in a carbon matrix is also a major factor affecting the uniformity of Li deposition, especially under long-term cycling or plating/stripping at high current density rates. The strong interaction energy between N and Li can change the carbon-nitrogen bond length during long-term cycling, resulting in the formation of lithium nitride (Li_3N) [145]. This will lead to the formation of a lithiophobic carbon matrix and the loss of active Li. As a result, there will be rapid capacity fading, large overpotentials, and low CE in the battery performance. A solution to this issue is to further introduce single metal atoms into the N-doped porous carbon Li host materials. The moderate interaction energy between Li and metal atoms embedded in N-doped carbon exhibits better stability of the atomic structure, preventing the loss of active materials and enhancing the cycling stability. There are several reports on co-doping of N and metal, N, and metal oxides or nitrides. A simple, one-step approach to creating a co-doped porous carbon framework is the carbonization of MOFs [157,179–181]. The synergy of conductivity by carbonization and lithiophilicity by metal and N-doping is expected to effectively regulate the Li nucleation sites leading to uniform Li deposition.

Zhai et al. designed single-atom metals supported on the N-doped graphene (SAM-NG) matrix as Li hosts, where M = Ni, Pt, Cu [145]. The metal atoms coordinated with nitrogen atoms on the layered graphene matrix increase the Li binding energy, inhibiting structural damage and encouraging uniform, dendrite-free Li deposition for long-term plating/stripping cycles. The pristine graphene (PG) and N-doped graphene (NG) showed cracks on the SEI film and larger Li metal islands projecting out from the Li host, respectively. At higher current densities, the difference in the surface morphology is more pronounced. The SAM-NG electrode prepared with Ni (SANi-NG) exhibited smooth Li deposition morphology with no obvious cracks and Li dendrites while the NG electrode showed dendritic Li growth with large dead Li particles. As a result, the SANi-NG electrode showed longer stable cycling stability with higher CE. It was calculated that the Li adsorption energy for PG, NG, and SANi-NG was 1.23 eV, 3.02 eV, and 1.92 eV, respectively, using Li adsorption energy mappings. If the Li adsorption of the host material is higher than the cohesive energy of Li (1.63 eV), Li nucleates on the surface of the host material, instead of forming bulk Li. Figs. 6f-h illustrate the Li-ion adsorption configurations on PG, NG, and SANi-NG structures. Thus, NG and SANi-NG can enable a sufficient nucleation site than PG, resulting in dendrite-free smooth Li deposition. Besides, the electronegativity of different materials such as Li (0.98), C (2.54), N (3.04), and Ni (1.91) dictates the Li adsorption activity. Figs. 6i-k show electron transfer from Li to PG, NG, and SANi-NG electrode, respectively. The electrode SANi-NG demonstrates the highest Li adsorption due to the smallest electronegativity of Li. In NG, a higher Li adsorption can be attributed to the strong N-Li bond, because N and Li have a large electronegativity difference. Nevertheless, this strong N-Li bond could lead to atomic structural damage between N-atoms and C-atoms. Liu et al. designed graphitic carbon-encapsulated Co nanoparticles (NP), and N-doped in their carbon skeleton designated as Co/N-PCNSs (Fig. 6l) as two-in-one hosts both for LiMA and sulfur (S) cathodes [180]. This helps to protect the LiMA anode and also enables high sulfur utilization with inhibition of lithium polysulfides shuttling effect.

The density functional theory (DFT) calculations were done to analyze the charge density and binding energy to understand the interaction between the Li-ion and heteroatom or N-doping [182,183]. Lee et al. studied the DFT calculations to understand the stable configurations of Li interstitial atoms in various N-graphitic structures [182]. They observed that pyridinic N exhibits higher Li adsorption energy (-6.12 eV) than pyrrolic N (-5.907) and quaternary N (-5.084 eV). To lower the Li interstitial formation energy, the heteroatom doping or N-doping into the porous carbon is an effective strategy. As a result, Co-embedded N-doped mesoporous graphite derived from bimetallic ZIF (Zn/Co) showed improved electrochemical cycling performance. Due to saturated electron orbitals, the carbon atom in a six-membered ring cannot provide additional electrons for Li-ion adsorption, resulting in weak interaction between them [183]. In contrast, the defects, edges or high coordination site due to N-doping replace the carbon atoms in a six-membered ring with N-atom. The N atom in graphitic-N forms a pi bond, providing extra electrons which leads to the increased charged density or conductivity. Further, pyrrolic N-atom replaces additional two carbon atoms. The lone pair containing pyrrolic-N acts as a Lewis base, strongly absorbing the Lewis acidic Li-ion. These results obtained from the simulation studies matches well with the XPS results. As a result, protected LiMA with N-doped CNT protected LiMA enable uniform distribution of Li-ion, resulting a high CE of ~ 99% over 500 h at a high current density of 8 mA cm^{-2}.

The synergy of fast electron transport, the high electronegativity of N-atoms with extra electrons from Co, and rearrangement between Co nanoparticles and N-doped graphene render uniform Li-ion flux and lithiophilic site for dendrite-free Li deposition. Liu et al. atomically dispersed CoN_x into graphene as a Li host to obtain strong lithiophilicity. As a result, a high CE of 99.2% was achieved at a current density of 2 mA cm^{-2} (~ 400 cycles) to achieve a capacity of 2 mAh cm^{-2}. Moreover, the hierarchical porous network lowers the effective current density, provides sufficient large space for Li accommodation, and alleviates the volume expansion of Li during Li plating/stripping cycles. Guo et al. designed lithiophilic Co/Co_4N NP embedded in hollow N-doped carbon nanocubes as Li host which displays high CE of 98.5% over 300 cycles and dendrite-free Li deposition and long-term cycling performance in high energy density Li-air battery [157]. Fig. 6m shows the schematic of the Li-air battery with lithiated Co/Co_4N NP embedded hollow N-doped carbon nanocubes. The high content of N and Co NP not only ensures lithiophilic and uniform distribution of the nucleation site but also stores store sufficient Li through the intercalation reaction of Co species and electroplating of Li into the porous structure.

3.4. Free-standing carbon electrode

It is challenging to create high-energy-density batteries using conventional metal current collectors such as Cu, Ni, Ti, and stainless steel due to the high-mass-density of these materials. The high cost and complexity of fabricating metal-based Li host/current collectors have motivated the search for free-standing conductive, flexible, and lithophilic porous carbons to replace these metals. The facile and low-cost production of carbon-based materials with various dimensions and hierarchical nanostructures is possible due to its flexibility and controllable mechanical properties. The incorporation of electrically conductive carbon which can function as both Li host and current collector is a promising method for further realization of LiMA. Employing conductive carbon as a free-standing Li host eliminates the need for a metal current collector. The use of an electrically conductive, lithiophilic, flexible, and free-standing light-weight 3D carbon matrix is an effective approach to minimize the volume expansion issues, reduce the effective local current density and provide sufficient space for Li accommodation. This reduces Li dendrite growth and improves interface stability. Porous, sp^2-hybridized carbon scaffolds such as CNT, CNF, and graphene have high electrical conductivity and excellent chemical and mechanical stability making these materials highly attractive as free-standing Li hosts [184,185]. The free-standing carbon electrode with high graphitization ensures high electrical conductivity. Besides, an ideal carbon-based Li host or current collector requires the lowest mass density and an optimized pore volume and porosity [59,60,164,186–191]. If the pore volume and surface area are too high, this may reduce battery performance. For instance, the unnecessarily large pore volume of carbonaceous materials may form an unstable SEI film resulting in the continuous consumption of both Li and electrolyte to compensate for the loss of SEI. The interconnected structure could collapse during repeated Li plating/stripping cycles, leading to the failure of the host material. Table 2 shows some representative structural and electrical properties of the free-standing carbon used as Li host and current collector. Cui et al. demonstrated that porous CNF (PCNF) with a specific surface area of 126.4 m^2 g^{-1}, the electrical con-

Table 2
Structural and electrical property of the free-standing carbon.

3D Carbon structure	Electrical conductivity (S m^{-1})/ Specific surface area (m^2 g^{-1}) & I_G/I_D	Pore size/pore volume (cm^3 g^{-1})	CE/N: cd/capacity	Ref.
MSP-20	-/2110/0.98	< 2 nm/1	90/5:1/1	[64]
CMK-3	-/1120/0.96	3.4 nm/1.3	>95/200:1/1	
graphene	$7.81^{*}10^{-5}$/-/-	10 nm/1.6	97/100: 0.5/0.5	[117]
ONPCGs	-/2396/-	2.18 nm/1.3	>99%/350:2/2	[168]
CNTs-decorated carbon sponge	9960 /~408/-	0.25/-	95.8/40:5/10	[199]
Hollow carbon fibers	-/140.1/0.93	0.6–2.5 nm/$1.83^{*}10^{-2}$ cm^3 cm^{-2}	~99.5/350:0.5/2	[65]
PCNF-0.5-HNO_3	127 /126.4/-	2.5–4 nm/0.23	96.6/~125:1/1	[166]
Fibrous carbon-N-graphene foam	9.6 Ω /482.16/-	2.13 nm/0.27	98.2/150:1/4	[141]
Carbon cloth	6700 /0.294/1.19	-/2.09	-/200:5/5 (ST)	[66]
CNF-TiN	755/412.4/-	2.04/0.211	95.8/300:1/1	[156]
CS-CNT	-/272/-	40 nm(CNT) /0.67	98.8/500:0.5/1	[200]
CS	-/123/-	< 40 nm/0.34	~94/55:0.5/1	
g-microtube	10,000/12/No D-peak	~1 μm/-	97.5/100:5/10	[67]
UGF	-	~ 400 μm/-	~50/~90:1/-	
AgNW-Graphene	440,000/19.9/	3 μm/4.95	97/50:0.5/1	[63]
CF	-/-/-	30–60 μm	3.25 mAh cm^{-2}–0.1C-100 cycles	[158]
GCF	-/0.37/0.86	≈72 μm/0.04 cm^3 cm^{-2}	98/50:0.53/8	[68]

ductivity of 1.27 S $cm^{-1,}$ and pore volume of 0.228 cm^3 g^{-1} results in the smallest nucleation overpotential of 32.1 mV with an exceptional energy density of 385 Wh kg^{-1} at the 100th cycles in Li-S batteries [166]. Increasing these parameters with a higher precursor ratio during material synthesis leads to rapid capacity failure and low CE. Benefitting from the electronic conductivity, mechanical flexibility, structural and chemical stability, hierarchical 3D nanostructured porosity, and low-cost, carbon has been successfully realized in LiMBs [192]. Free-standing porous carbon can be employed as Li host/current collector by making C/Li composite in a variety of methods such as Li electroplating, molten Li infusion, and mechanical pressing. However, the lithiophobic surface of the porous carbon matrix cannot promote uniform Li deposition at a high current density and high Li plating capacity. The lattice mismatch between the body-centered cubic structured Li metal and hexagonal structured carbon leads to a poor affinity of carbon towards Li. As a result, the initial Li deposition and plating/stripping at higher current densities nucleates poorly leading to non-uniform and dendritic Li deposition during subsequent Li plating cycles. These sparse Li agglomerates lead to the loosely connected Li deposition increasing the possibility of dead Li formation. With these considerations in mind, various surface modifications of porous carbon with lithiophilic materials have been investigated using methods including Li electroplating [152,166,171], molten Li infusion [121,139,159,164,173,193-197], and mechanical roll press methods [158,198]. As a result, smooth Li electrodeposition and uniform insertion of molten Li into the porous structure can be obtained.

In the electroplating method, free-standing electrodes are considered as the working electrode and Li foil as the counter/reference electrode, and then the electrochemical performance such as the symmetrical cell test (ST) and CE test is evaluated. For practical full cell testing, a sufficient amount of Li is electroplated on the free-standing 3D porous carbon, and the battery is disassembled. The electroplated carbon electrode is cleaned to remove residual Li salts and electrolyte, and then coupled with a cathode to fabricate a full cell [44,67,68,199,201,202]. This results in the complex processing of electrode fabrication for practical LiMBs. Besides, it is still challenging to obtain uniform Li electroplating because the short Li-ion diffusion path leads to the deposition of Li on the outer surface of the Li host [83]. Thus, the development of an electroplated C/Li composite anode still suffers from high cost, uncontrolled and uneven Li distribution, and time-consuming fabrication.

Pre-storing of molten Li into the free-standing porous electrode is a promising technique for making C/Li composites because it predefines the Li anode space and provides sufficient Li for high-energy-density batteries [203]. The direct infusion of molten Li into such porous structures can avoid the complexity of dissembling the batteries before fabricating a full cell. Lin et al. reported lithiophilic layered reduced graphene oxide (rGO) to restore or infuse Li into the uniform nanoscale interlayer gaps [121]. The synergy of lithiophilicity and capillary force generated by the nanogaps in rGO imparts a high Li wettability. Figs. 7a-c show an SEM image of densely stacked pristine graphene oxide (GO), sparked rGO, and layered Li-rGO, respectively. The inset of Fig. 7c shows a Li-rGO strip coiled around a glass rod, illustrating the good flexibility. Fourier transform infrared (FTIR) spectroscopy measurements confirm the reduction of GO by the spark reaction (Fig. 7d). The presence of –OH peak in GO has disappeared in rGO. The XPS analysis also confirms the significant reduction in O 1 s signal and C-O-H peak. The molten Li-infused lithiophilic and flexible rGO shows ~20% dimensional change during cycling and reduced overpotential in the ester-based electrolyte. Zhang et al. designed a highly conductive, free-standing carbon with well-aligned porous channels as a Li host material [193]. The C/Li composite was prepared by pre-storing molten Li into lithiophilic, ZnO-coated carbonized wood as shown in Fig. 7e. This C/Li composite anode demonstrated a high capacity of 2650 mAh g−1 and excellent long-term cycling performance even at a high current density of 3 mA cm−2 with reduced overpotential. Zhang et al. demonstrated a coralloid carbon fiber (CF) by electroplating silver (Ag) on CFs [173]. Fig. 7f shows a schematic illustration of preparing carbon fiber/Ag-Li composite materials from CF. The lithiophilic Ag was coated on the CF before infusing the molten Li into the CF matrix. Fig. 7g shows SEM images with digital photos in the inset for CF, Ag-decorated CF, and CF/Ag-Li composites. The CF/Ag-Li (I) is the composite with surface Li infusion and CF/Ag-Li (II) is the composite with molten Li in the porous framework. Electroplating can be a more facile and cost-effective approach for obtaining lithiophilic property on porous carbon compared to chemical vapor deposition, sputtering, or atomic layer deposition. The lithiophilic nucleation sites uniformly wet the surface with molten Li to achieve CF/Ag-Li composite. The symmetrical cell test demonstrated long-term stable plating/stripping cycles with low voltage hysteresis at a high current density of 10 mA cm−2 and to achieve a high capacity of 10 mAh cm−2. The CF/Ag-Li composite anode paired with S-cathode achieved capacity retention of 64.3% at 0.5 C even after 400 cycles.

The infusion of molten Li into nano/microstructured carbon at high-temperature and the electrodeposition of Li into porous carbon can be risky and complex. Besides, the infusion of molten Li into a porous carbon framework demands a thick and heavy, free-standing electrode, which is not considered suitable for practical high-energy-density batteries. As an alternative to the thermal infusion of molten Li and electroplating methods, a rolling press method has been recently reported as a simple and scalable mechanical technique to fabricate Li composites [100,204–206]. The fabrication of C/Li composites provides excellent mechanical & chemical strength under the redox environment and high

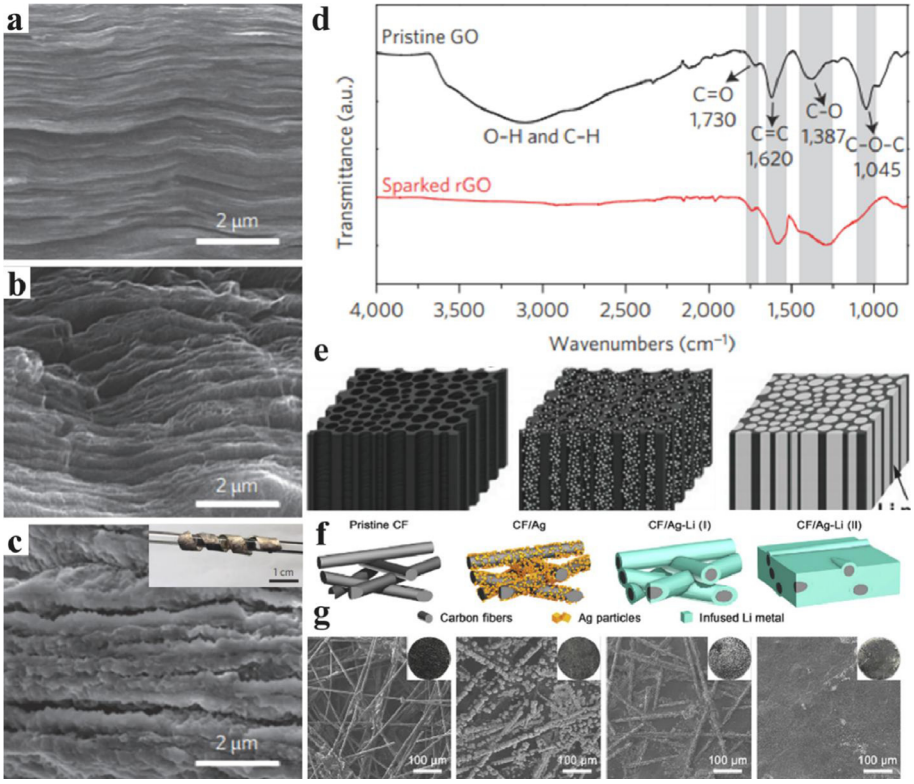

Fig. 7. a-c SEM images of pristine GO film, layered rGO, and Li-rGO composite film. d FTIR spectrum of pristine GO and sparked rGO layer. Reproduced with permission from Ref. [121], Springer Nature. e Schematics of the C/Li composite preparation process from C-wood after ZnO coating and molten Li infusion. Reproduced with permission from Ref. [193], Proceedings of the National Academy of Sciences. **f** Schematic of the preparation steps of carbon fiber/Ag-Li composite. g Corresponding SEM images and the inset: digital photos. Reproduced with permission from Ref. [173], Elsevier.

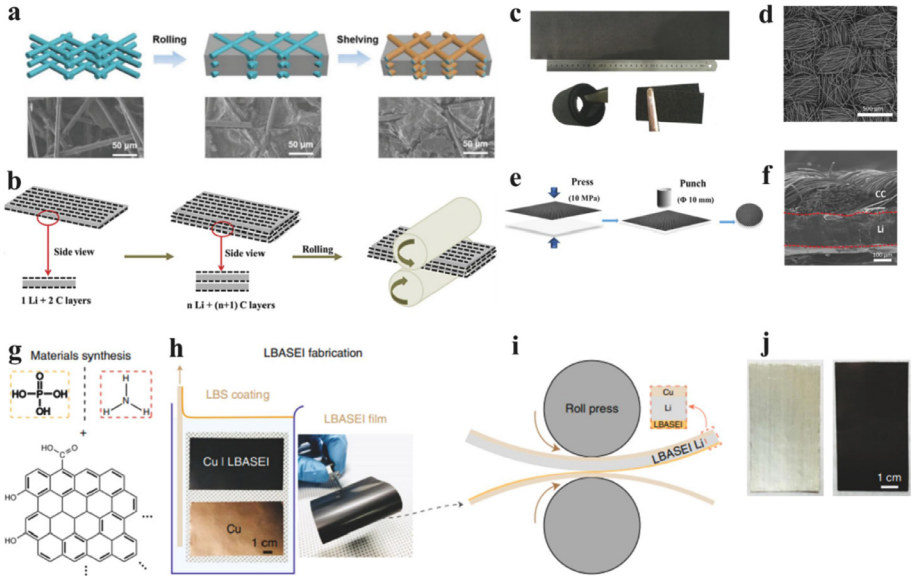

Fig. 8. **a** Schematic demonstration and corresponding SEM images of pristine CF, CF/Li composite after roll-press, and shelving for 72 h. Reproduce with permission from Ref. [158], John Wiley and Sons. **b** Schematic illustration of C/Li composite anode by a roll-press method. Reproduced with permission from Ref. [210], Elsevier. **c** Optical image and folding property of carbon cloth. **d** Top-view SEM image of carbon cloth. **e** the synthesis steps of C/Li composite anode by applying pressure. **f** Cross-sectional SEM image of C/Li composite anode. Reproduced with permission from Ref. [66], Elsevier. **g** Molecular structure of phosphoric acid and ammonia gas precursor. **h,i** LBASEI fabrication process by LBS method and transfer of LBASEI from Cu to produce LBASEI/Li composite by roll press method. **j** Digital photos of pristine Li and LBASEI/Li. Reproduced with permission from Ref. [198], Springer Nature.

energy density due to the low density of carbon. Although the Li wettability of the carbon host materials may not be needed while making the composites, the interaction of Li-ions and lithiophilic materials can govern the Li deposition curing plating/stripping cycles. Li metal has excellent malleability even at room temperature, and this property facilitates the easy production of C/Li composite anode by pressing, roll-in or folding methods [66,158,205,207,208]. Besides the advantages of flexible, conducting, and lithiophilic carbon, lithium offers a very low-density of 0.53 g cm^{-3} and excess Li-ion source. Moreover, the high mechanical strength of carbon host materials can endure the high pressures required to manufacture such composites [209].

Shi et al. fabricated carbon fiber/Li composite materials through a one-step rolling method at room temperature [158]. Fig. 8a shows a schematic illustration and corresponding SEM images of pristine CF, CF/Li composite after roll-press, and shelving for 72 h. The thin lithiophilic LiC_6 layer, which enhances the wettability of the carbon fiber was formed between the carbon fibers and the metallic Li due to an *in-situ* intercalation reaction between Li and C. The C electronegativity is increased due to electron transfer from Li upon intercalation. As a result, the formation of lithiophilic LiC_6 increases the interaction between the carbon framework and Li-ions. The Gibbs free energy of the intercalation reaction (-10.59 kJ mol^{-1}) indicates that this is the reaction is spontaneous once the Li metal and carbon fiber come into contact. This demonstrates that a one-step rolling method is appropriate for the large-scale carbon fiber/Li composite to revive the LiMA for practical high-energy-density. Shu et al. fabricated C/Li composites by sandwiching Li between

Table 3
Symmetrical cell performance based on C/Li composite.

carbon matrix	fabrication method	symmetrical cell performance	Ref.
Graphitized CF	Electroplating	2 mA cm^{-2} for 0.5 h - 300 h/Ether	[68]
3D carbon paper	Electroplating	2 mA cm^{-2} for 1 h - 1000 h/Ether	[211]
Ag- 3D graphene	Electroplating	40 mA cm^{-2} for 1.5 min - 50 h/Ether	[63]
CNF-TiN	Electroplating	4 mA $cm^{-2}$for 15 min - 100 h/Ether	[156]
Graphite microtube	Electroplating	1 mA cm^{-2}-for 10 h - 3000 h/Ether	[67]
N-CNTs decorated carbon sponge	Electroplating	15 mA cm^{-2} for 1 h - 600 h/Ether	[199]
CNT on porous carbon cloth	Molten Li infusion	5 mA cm^{-2} for 1 h - 500 h/Ether	[212]
TiC/C	Molten Li infusion	3 mA cm^{-2} for 20 min - 200 h/Ester	[159]
Ag-Coralloid carbon fibers	Molten Li infusion	1 mA cm^{-2} for 1 h - 400 h/Ether	[173]
ZnO@carbon cloth	Molten Li infusion	10 mA cm^{-2} for 3 min - 30 h/Ester	[197]
3D nanoporous N-graphene	Molten Li infusion	1 $mAcm^{-2}$ for 1 h - 1454 h/Ether	[164]
	Molten Li infusion	3 mA cm^{-2} for 20 min - 250 h/Ester	[193]
carbon fiber/Li	Mechanical press	5 mA cm^{-2} for 1 h - 90 h/Ether	[158]
rGO/Li/rGO	Mechanical press	10 mA cm^{-2} for 1 h - 1500 h/Ether	[210]
Li/carbon fiber/Li	Mechanical press	1 mA cm^{-2} for 1 h - 950 h/Ester	[205]
Li/carbon cloth/Li	Mechanical press	5 mA cm^{-2} for 12 min - 80 h/Ester	[66]
PrGO/Li	Mechanical press	1 mA cm^{-2} for 1 h - 400 h/Ester	[198]
CNT/Li	Mechanical mix	0.5 mA cm^{-2} for 1 h - 30 h/Ether	[207]

carbon layers of rGO, activated microwave exfoliated GO (aMEGO), and activated carbon through the rolling press method as shown in Fig. 8b [210]. The thickness of the C/Li composite was maintained at 100 μm and 460 μm based on the number of Li and carbon layers, keeping in mind the rolling hardening of Li. Zhou et al. designed carbon cloth/Li composite through a facile, one-step method by applying 10 MPa pressure to a stack of carbon cloth placed over the Li [66]. Figs. 8c,d show photographs of the commercially available carbon cloth and a top-view SEM image of the carbon cloth. Fig. 8e shows the one-step process of stacking the carbon cloth with the Li foil by applying pressure. Fig. 8f shows a cross-sectional SEM image of well-attached carbon cloth on top of the Li foil. The carbon cloth/Li composite anode paired with both $Li_4Ti_5O_{12}$ (LTO) and $LiNi_5Co_2Mn_3O_4$ (NCM) cathode exhibited long and stable cycling performance. Kim et al. used Langmuir-Blodgett artificial SEIs (LBASEIs) to functionalize the rGO with phosphate (PrGO) and ammonia (NrGO) in a facile and scalable production process to stabilize the LiMA [198]. Fig. 8g shows the molecular structures of phosphoric acid and ammonia gas. Functionalizing rGO with phosphorus or ammonia allows nanoscale thickness control and provides an easy and scalable method for fabricating the ASEI. Figs. 8h,i show the fabrication process of LBASEI on Cu foil by the Langmuir–Blodgett scooping (LBS) method and transfer of the LBASEI on Li foil by the roll-press method, respectively. Fig. 8j shows digital photographs of pristine Li metal and the LBASEI-Li composite. The pairing of a Li/PrGO composite anode with an NCM (811) cathode delivered stable cycling of more than 120 cycles with an energy density of 260 Wh kg^{-1}. Table 3 shows some representative symmetrical cell performance of C/Li composite based on their structures and fabrication methods.

To further improve the Li plating/stripping behavior and realize a stable and safe LiMA, the development of in-situ or ex-situ SEI on mechanical roll-press C/Li composite anode has been considered as an effective approach [112,205,207,213]. The tailor-designed SEI effectively provides a physical barrier between the C/Li composite and the liquid electrolyte to prevent side reactions and suppress Li-dendrite growth. Fig. 9a shows a schematic illustration of the engineered C/Li composite followed by the SEI generation process. The C/Li composite anode with SEI on top and carbon fiber matrix on the bottom ("housed Li") showed a stable structure and fast Li-ion/electron transport. Fig. 9b shows the stable long-term pouch cell cycling performance at 0.5 C after one cycle at 0.05 C using housed Li as the anode and LiFePO4 as the cathode. Guo et al. fabricated a CNT/Li composite with ASEI via molecular self-assembly monolayer of octadecyl phosphonic acid (OPA) to accommodate the volume expansion of Li during plating/stripping and protect the composite anode from side reactions with the electrolyte and air [207]. The CNT/Li+ SEI composite anode coupled with CNT microspheres (CNTm) O2 cathode demonstrated improved electrochemical reversibility i.e., the O2 recovery efficiency of 95% for more than 90 cycles. The SEI-developed C/Li composite anode showed highly reversible CE with stable cycling performance, which was further improved using CNTm even at higher current densities as shown in Figs. 9c-e.

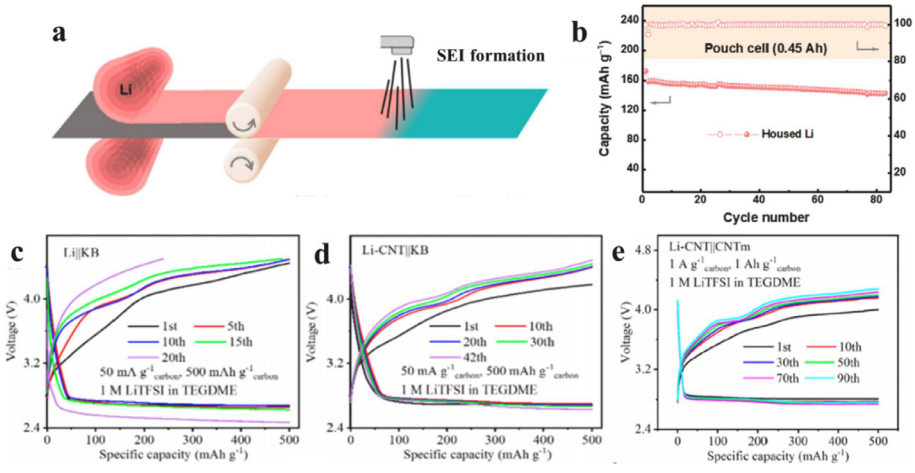

Fig. 9. **a** Schematic illustration of SEI formation on C/Li composite developed by the roll-press method. **b** Full cell cycling performance in pouch cell using LiFePO4 as a cathode and SEI-protected C/Li composite anode. Reproduced with permission from Ref. [205], Elsevier. **c-e** Voltage profile of Li-O_2 cell using Li/KB, Li-CNT/KB, and Li-CNT/CNTm configuration. Reproduced with permission from Ref. [207], American Chemical Society.

4. Conclusion and perspectives

Lithium metal-based batteries which offer the advantage of higher energy density compared to conventional graphite-based anode batteries have been pursued for many years. The lithium metal anode (LiMA) is considered a key component for next-generation batteries potentially offering energy densities of > 500 Wh kg^{-1} at the cell level to drive the energy storage market for electric vehicles. However, the practical application of LiMA is hindered by the high chemical reactivity and the high-volume expansion of Li that lead to uncontrolled side reactions, Li dendrite growth, and the formation of an unstable SEI. The C/Li composite anode has demonstrated discernable progress with flooded electrolyte excess Li (> 50 mAh cm^{-2}), high ratio of negative electrode capacity to positive electrode capacity (N/P >3), and charge/discharge at a low current density (< 1 mA cm^{-2}). However, key challenges remain with C/Li composite anodes including the mitigation of the large volume expansion and high chemical reactivity of Li. There is still a need to illustrate the feasible pathways for high-energy, stable, and long-cycling LiMBs with lean lithium (< 10 mAh cm^{-2} or < 50 μm), low N/P (< 2), lean electrolyte or low electrolyte to capacity ratio (< 3 g $(Ah)^{-1}$) and high current density (> 3 mA cm^{-2}). The limited Li/3D carbon composites fabricated by electroplating, molten Li infusion, and mechanical roll-press methods overcome significant limitations of the LiMA. The introduction of highly conductive and lithiophilic free-standing electrodes has proven to be the best candidate as both Li host and current collector for reviving the LiMBs. The initial focus should target safety, high-energy density, and long-term stable battery performance. Moreover, the use of 3D porous carbon as both Li host and current collector will reduce the size, weight, and cost. The advantages of well-designed micro/nanostructured C/Li composite could effectively improve the safety issues and enhance the battery performance due to: (1) high surface area of carbon provides sufficient space for Li accommodation, (2) significantly lower effective current density, (3) mechanical and chemical stability to provide high stability during long-term cycling (4) reduced weight with good flexibility to increases the energy density and stabilize the electrode/electrolyte SEI, and (5) reduce the cost of processing and material cost. This improved reliability of LiMA batteries and success in these Li/3D carbon composite will open new opportunities and make them appealing for large-scale energy applications. The key technical issues associated with C/Li composite anodes are listed below to serve as a roadmap for academic and industrial partners to reach the goal of practical, high-energy-density batteries.

(1) The deeper understanding of the *in-situ* SEI formation on carbon/Li composite anode and Li plating/stripping behavior by state-of-art characterization tools [214–217] such as synchrotron X-ray analytical techniques, cryogenic electron microscopy, XPS, time of flight secondary ion mass spectrometry (TOF-SIMS), Fourier transform infrared spectroscopy (FTIR), atomic force microscopy (AFM, transmission electron microscopy (TEM), cryo-TEM, enhanced Raman spectroscopy, auger electron spectroscopy (AES) are critically important to understand the morphology, chemical composition, and Li-ion transport behavior during and/or after plating/stripping. The simulation techniques [147,218–225] such as the finite Peled model, Mosaic model, coulombic interaction mechanism model, element method, phase field theory, molecular dynamics, first-principle density functional theory are also equally essential to verify the experimental results and provide insight into the new ideas on the different status of SEI. Besides, the complex reaction mechanism across the interface of 3D porous carbon/Li composite and the liquid electrolyte/solid electrolyte, the transport of charges such as positive Li-ion, partially positive Li-ion, and electron need to be explored further.

(2) The key factors such as lithiophilicity and conductivity in host materials play an important role in Li nucleation and deposition behavior. The different interactions which induce the Li nucleation depending upon the lithiophilic functional group, heteroatom, or other polar atoms need to be understood in detail. Due to higher mass loading of cathodes and charge/discharge for higher capacity, the lithiophilic materials may be covered, resulting in the formation of non-uniform and mossy Li. Further advancement such as a composite of flexible polymer and lithiophilic carbon host may confine the Li within the 3D porous structure.

(3) In addition to the lightweight, conductive, and lithiophilic 3D porous carbon/Li composite anode, the artificial ultrathin, and flexible, highly mechanical, and chemical stable *ex-situ* SEI are desired to separate the hyperactive LiMA and liquid electrolyte.

(4) The use of solid-state electrolyte is a promising strategy to provide safety and higher energy density compared to flammable liquid organic electrolyte [226–229]. Moreover, replacing planar Li with Li/3D porous carbon composite anode is capable to lower the impedance and interface incompatibilities under high areal capacity and current density [44,230].

Declaration of Competing Interest

The authors declare no competing interest.

Acknowledgments

This work has been supported by SDBoR Competitive Grant Program, NSF MRI (1428992), NASA EPSCoR (NNX15AM83A), SDBoR R&D Program, and EDA University Center Program (ED18DEN3030025). A.M. and J.E. was supported as part of the Center for Electrochemical Energy Science, an Energy Frontier Research Center funded by the U.S. Department of Energy, Office of Science, Office of Basic Energy Sciences.

References

[1] D. Lin, Y. Liu, Y. Cui, Reviving the lithium metal anode for high-energy batteries, Nat. Nanotechnol. 12 (3) (2017) 194.
[2] S. Li, M. Jiang, Y. Xie, H. Xu, J. Jia, J. Li, Developing high-performance lithium metal anode in liquid electrolytes: challenges and progress, Adv. Mater. 30 (17) (2018) 1706375.
[3] X.C. Ren, X.Q. Zhang, R. Xu, J.Q. Huang, Q. Zhang, Analyzing energy materials by cryogenic electron microscopy, Adv. Mater. (2020) 1908293.
[4] Z. Zhao, R. Pathak, X. Wang, Z. Yang, H. Li, Q. Qiao, Sulfiphilic FeP/rGO as a highly efficient sulfur host for propelling redox kinetics toward stable lithium-sulfur battery, Electrochim. Acta 364 (2020) 137117.
[5] Z. Zhao, et al., Synergetic effect of spatially separated dual co-catalyst for accelerating multiple conversion reaction in advanced lithium sulfur batteries, Nano Energy 81 (2021) 105621.
[6] R. Pathak, et al., Fluorinated hybrid solid-electrolyte-interphase for dendrite-free lithium deposition, Nat. Commun. 11 (1) (2020) 1–10.
[7] R. Pathak, et al., Ultrathin bilayer of graphite/SiO2 as solid interface for reviving Li metal anode, Adv. Energy Mater. 9 (36) (2019) 1901486.
[8] J.-M. Tarascon, M. Armand, in: Issues and Challenges Facing Rechargeable Lithium batteries," in Materials for Sustainable Energy: A Collection of Peer-Reviewed Research and Review Articles from Nature Publishing Group, World Scientific, 2011, pp. 171–179.
[9] Y. Cao, M. Li, J. Lu, J. Liu, K. Amine, Bridging the academic and industrial metrics for next-generation practical batteries, Nat. Nanotechnol. (2019) 1.
[10] J. Liu, et al., Pathways for practical high-energy long-cycling lithium metal batteries, Nat. Energy 4 (3) (2019) 180–186.
[11] Y. Chen, et al., Li metal deposition and stripping in a solid-state battery via Coble creep, Nature 578 (7794) (2020) 251–255.
[12] T.K. Schwietert, et al., Clarifying the relationship between redox activity and electrochemical stability in solid electrolytes, Nat. Mater. 19 (4) (2020) 428–435.
[13] Q. Zhao, S. Stalin, C.-Z. Zhao, L.A. Archer, Designing solid-state electrolytes for safe, energy-dense batteries, Nat. Rev. Mater. (2020) 1–24.
[14] Y. Zhou, et al., Real-time mass spectrometric characterization of the solid—electrolyte interphase of a lithium-ion battery, Nat. Nanotechnol. 15 (3) (2020) 224–230.
[15] J. Lang, et al., High-purity electrolytic lithium obtained from low-purity sources using solid electrolyte, Nat. Sustain. (2020) 1–5.
[16] J. Wan, et al., Ultrathin, flexible, solid polymer composite electrolyte enabled with aligned nanoporous host for lithium batteries, Nat. Nanotechnol. 14 (7) (2019) 705–711.
[17] R. Pfenninger, M. Struzik, I. Garbayo, E. Stilp, J.L. Rupp, A low ride on processing temperature for fast lithium conduction in garnet solid-state battery films, Nat. Energy 4 (6) (2019) 475–483.
[18] T. Famprikis, P. Canepa, J.A. Dawson, M.S. Islam, C. Masquelier, Fundamentals of inorganic solid-state electrolytes for batteries, Nat. Mater. (2019) 1–14.

[19] N. Wu, et al., In Situ formation of Li3P layer enables fast Li+ conduction across Li/solid polymer electrolyte interface, Adv. Funct. Mater. 30 (22) (2020) 2000831.
[20] X.-B. Cheng, et al., Implantable solid electrolyte interphase in lithium-metal batteries, Chem 2 (2) (2017) 258–270.
[21] J. Chen, et al., Electrolyte design for LiF-rich solid–electrolyte interfaces to enable high-performance microsized alloy anodes for batteries, Nat. Energy 5 (5) (2020) 386–397.
[22] N.W. Li, Y.X. Yin, C.P. Yang, Y.G. Guo, An artificial solid electrolyte interphase layer for stable lithium metal anodes, Adv. Mater. 28 (9) (2016) 1853–1858.
[23] D. Chen, et al., In situ preparation of thin and rigid COF film on Li anode as artificial solid electrolyte interphase layer resisting Li dendrite puncture, Adv. Funct. Mater. 30 (7) (2020) 1907717.
[24] Z. Wang, et al., Building artificial solid-electrolyte interphase with uniform intermolecular ionic bonds toward dendrite-free lithium metal anodes, Adv. Funct. Mater. (2020) 2002414.
[25] P. Zhai, et al., In situ generation of artificial solid-electrolyte interphases on 3d conducting scaffolds for high-performance lithium-metal anodes, Adv. Energy Mater. 10 (8) (2020) 1903339.
[26] K. Tang, et al., A stable solid electrolyte interphase for magnesium metal anode evolved from a bulky anion lithium salt, Adv. Mater. 32 (6) (2020) 1904987.
[27] S.K. Cho, et al., Printable solid electrolyte interphase mimic for antioxidative lithium metal electrodes, Adv. Funct. Mater. (2020) 2000792.
[28] F. Liu, et al., A mixed lithium-ion conductive Li2S/Li2Se protection layer for stable lithium metal anode, Adv. Funct. Mater. 30 (23) (2020) 2001607.
[29] X. Ni, T. Qian, X. Liu, N. Xu, J. Liu, C. Yan, High lithium ion conductivity LiF/GO solid electrolyte interphase inhibiting the shuttle of lithium polysulfides in long-life Li–S batteries, Adv. Funct. Mater. 28 (13) (2018) 1706513.
[30] S. Li, W. Zhang, J. Zheng, M. Lv, H. Song, L. Du, Inhibition of polysulfide shuttles in Li–S batteries: modified separators and solid-state electrolytes, Adv. Energy Mater. (2020) 2000779.
[31] J. Wu, et al., Ultralight layer-by-layer self-assembled MoS2-polymer modified separator for simultaneously trapping polysulfides and suppressing lithium dendrites, Adv. Energy Mater. 8 (35) (2018) 1802430.
[32] Z. Hu, et al., Dendrite-free lithium plating induced by in situ transferring protection layer from separator, Adv. Funct. Mater. 30 (5) (2020) 1907020.
[33] C. Zhang, et al., Anion-sorbent composite separators for high-rate lithium-ion batteries, Adv. Mater. 31 (21) (2019) 1808338.
[34] K. Liu, et al., Extending the life of lithium-based rechargeable batteries by reaction of lithium dendrites with a novel silica nanoparticle sandwiched separator, Adv. Mater. 29 (4) (2017) 1603987.
[35] H. Lee, et al., Suppressing lithium dendrite growth by metallic coating on a separator, Adv. Funct. Mater. 27 (45) (2017) 1704391.
[36] M.S. Gonzalez, et al., Draining over blocking: nano-composite janus separators for mitigating internal shorting of lithium batteries, Adv. Mater. 32 (12) (2020) 1906836.
[37] Z. Zhou, et al., A multifunctional separator enables safe and durable lithium/magnesium–sulfur batteries under elevated temperature, Adv. Energy Mater. 10 (5) (2020) 1902023.
[38] M. Waqas, S. Ali, W. Lv, D. Chen, B. Boateng, W. He, High-performance PE-BN/PVDF-HFP bilayer separator for lithium-ion batteries, Adv. Mater. Interfaces 6 (1) (2019) 1801330.
[39] Y. Zhong, et al., Metal organic framework derivative improving lithium metal anode cycling, Adv. Funct. Mater. 30 (10) (2020) 1907579.
[40] W. Ren, Y. Zheng, Z. Cui, Y. Tao, B. Li, and W.J.E.S.M. Wang, "Recent progress of functional separators in dendrite inhibition for lithium metal batteries," 2020.
[41] Y. Guo, H. Li, T. Zhai, Reviving lithium-metal anodes for next-generation high-energy batteries, Adv. Mater. 29 (29) (2017) 1700007.
[42] L. Zhou, et al., Recent developments on and prospects for electrode materials with hierarchical structures for lithium-ion batteries, Adv. Energy Mater. 8 (6) (2018) 1701415.
[43] R. Zhang, N.W. Li, X.B. Cheng, Y.X. Yin, Q. Zhang, Y.G. Guo, Advanced micro/nanostructures for lithium metal anodes, Adv. Sci. 4 (3) (2017) 1600445.
[44] T.S. Wang, X. Liu, Y. Wang, L.Z. Fan, High areal capacity dendrite-free Li anode enabled by metal–organic framework-derived nanorod array modified carbon cloth for solid state Li metal batteries, Adv. Funct. Mater. (2020) 2001973.
[45] W. Deng, X. Zhou, Q. Fang, Z. Liu, Microscale lithium metal stored inside cellular graphene scaffold toward advanced metallic lithium anodes, Adv. Energy Mater. 8 (12) (2018) 1703152.
[46] Q. Song, et al., Vertically grown edge-rich graphene nanosheets for spatial control of Li nucleation, Adv. Energy Mater. 8 (22) (2018) 1800564.
[47] Q. Xu et al., "High energy density lithium metal batteries enabled by a porous graphene/MgF2 framework," vol. 26, pp. 73–82, 2020.
[48] R. Pathak, Y. Zhou, Q. Qiao, Recent advances in lithiophilic porous framework toward dendrite-free lithium metal anode, Appl. Sci. 10 (12) (2020) 4185.
[49] H. Lee, J. Song, Y.-J. Kim, J.-K. Park, H.-T. Kim, Structural modulation of lithium metal-electrolyte interface with three-dimensional metallic interlayer for high-performance lithium metal batteries, Sci. Rep. 6 (1) (2016) 1–10.
[50] D. Tian, et al., MoN supported on graphene as a bifunctional interlayer for advanced Li-S batteries, Adv. Energy Mater. 9 (46) (2019) 1901940.
[51] X.B. Cheng, et al., Dendrite-free lithium deposition induced by uniformly distributed lithium ions for efficient lithium metal batteries, Adv. Mater. 28 (15) (2016) 2888–2895.
[52] S. Kim, et al., The role of interlayer chemistry in Li-metal growth through a garnet-type solid electrolyte, Adv. Energy Mater. 10 (12) (2020) 1903993.
[53] L. Ren, A. Wang, X. Zhang, G. Li, X. Liu, J. Luo, Eliminating dendrites through dynamically engineering the forces applied during Li deposition for stable lithium metal anodes, Adv. Energy Mater. 10 (4) (2020) 1902932.
[54] K. Shen, et al., Magnetic field–suppressed lithium dendrite growth for stable lithium-metal batteries, Adv. Energy Mater. 9 (20) (2019) 1900260.
[55] K. Chen, et al., Flower-shaped lithium nitride as a protective layer via facile plasma activation for stable lithium metal anodes, Energy Storage Mater. 18 (2019) 389–396.
[56] S.H. Wang et al.,"Stable Li metal anodes via regulating lithium plating/stripping in vertically aligned microchannels," vol. 29, no. 40, p. 1703729, 2017.
[57] R. Zhang, et al., Conductive nanostructured scaffolds render low local current density to inhibit lithium dendrite growth, Adv. Mater. 28 (11) (2016) 2155–2162.
[58] R. Zhang, X. Shen, X.-B. Cheng, and Q.J.E.S.M. Zhang,"The dendrite growth in 3D structured lithium metal anodes: Electron or ion transfer limitation?," vol. 23, pp. 556–565, 2019.
[59] H.J. Peng, et al., Nanoarchitectured graphene/CNT@ porous carbon with extraordinary electrical conductivity and interconnected micro/mesopores for lithium-sulfur batteries, Adv. Funct. Mater. 24 (19) (2014) 2772–2781.
[60] M.K. Rybarczyk, H.-J. Peng, C. Tang, M. Lieder, Q. Zhang, M.-M. Titirici, Porous carbon derived from rice husks as sustainable bioresources: insights into the role of micro-/mesoporous hierarchy in hosting active species for lithium–sulphur batteries, Green Chem. 18 (19) (2016) 5169–5179.
[61] S. Luo, et al., A 3D conductive network of porous carbon nanoparticles interconnected with carbon nanotubes as the sulfur host for long cycle life lithium–sulfur batteries, Nanoscale 10 (47) (2018) 22601–22611.
[62] C. Chai, H. Tan, X. Fan, K. Huang, MoS2 nanosheets/graphitized porous carbon nanofiber composite: a dual-functional host for high-performance lithium–sulfur batteries, J. Alloys Compd. 820 (2020) 153144.
[63] P. Xue, et al., A hierarchical silver-nanowire–graphene host enabling ultrahigh rates and superior long-term cycling of lithium-metal composite anodes, Adv. Mater. 30 (44) (2018) 1804165.
[64] J. Jeong, J. Chun, W.-G. Lim, W.B. Kim, C. Jo, J. Lee, Mesoporous carbon host material for stable lithium metal anode, Nanoscale 12 (22) (2020) 11818–11824.
[65] L. Liu, et al., Free-standing hollow carbon fibers as high-capacity containers for stable lithium metal anodes, Joule 1 (3) (2017) 563–575.
[66] Y. Zhou, et al., A carbon cloth-based lithium composite anode for high-performance lithium metal batteries, Energy Storage Mater. 14 (2018) 222–229.
[67] S. Jin, et al., High areal capacity and lithium utilization in anodes made of covalently connected graphite microtubes, Adv. Mater. 29 (38) (2017) 1700783.
[68] T.T. Zuo, et al., Graphitized carbon fibers as multifunctional 3D current collectors for high areal capacity Li anodes, Adv. Mater. 29 (29) (2017) 1700389.
[69] K. Yan, et al., Ultrathin two-dimensional atomic crystals as stable interfacial layer for improvement of lithium metal anode, Nano Lett. 14 (10) (2014) 6016–6022.
[70] J. Xie, et al., Stitching h-BN by atomic layer deposition of LiF as a stable interface for lithium metal anode, Sci. Adv. 3 (11) (2017) eaao3170.
[71] Y. Liu, D. Lin, Z. Liang, J. Zhao, K. Yan, Y. Cui, Lithium-coated polymeric matrix as a minimum volume-change and dendrite-free lithium metal anode, Nat. Commun. 7 (2016) 10992.
[72] L. Fan, H.L. Zhuang, W. Zhang, Y. Fu, Z. Liao, Y. Lu, Stable lithium electrodeposition at ultra-high current densities enabled by 3D PMF/Li composite anode, Adv. Energy Mater. 8 (15) (2018) 1703360.
[73] C.-P. Yang, Y.-X. Yin, S.-F. Zhang, N.-W. Li, Y.-G. Guo, Accommodating lithium into 3D current collectors with a submicron skeleton towards long-life lithium metal anodes, Nat. Commun. 6 (1) (2015) 1–9.
[74] H. Zhao, et al., Compact 3D copper with uniform porous structure derived by electrochemical dealloying as dendrite-free lithium metal anode current collector, Adv. Energy Mater. 8 (19) (2018) 1800266.
[75] Q. Yun, et al., Chemical dealloying derived 3D porous current collector for Li metal anodes, Adv. Mater. 28 (32) (2016) 6932–6939.
[76] Y. An, et al., Vacuum distillation derived 3D porous current collector for stable lithium–metal batteries, Nano Energy 47 (2018) 503–511.
[77] Y. Shi, et al., A self-supported, three-dimensional porous copper film as a current collector for advanced lithium metal batteries, J. Mater. Chem. A 7 (3) (2019) 1092–1098.
[78] L.-L. Lu, et al., Free-standing copper nanowire network current collector for improving lithium anode performance, Nano Lett. 16 (7) (2016) 4431–4437.
[79] Y. Liu et al.,"Oxygen and nitrogen Co-doped porous carbon granules enabling dendrite-free lithium metal anode," vol. 18, pp. 320–327, 2019.
[80] K. Yan, B. Sun, P. Munroe, G. Wang, Three-dimensional pie-like current collectors for dendrite-free lithium metal anodes, Energy Storage Mater. 11 (2018) 127–133.
[81] S.H. Wang, et al., Stable Li metal anodes via regulating lithium plating/stripping in vertically aligned microchannels, Adv. Mater. 29 (40) (2017) 1703729.
[82] K. Chen, et al., A copper-clad lithiophilic current collector for dendrite-free lithium metal anodes, J. Mater. Chem. A 8 (4) (2020) 1911–1919.
[83] S.S. Chi, Y. Liu, W.L. Song, L.Z. Fan, Q. Zhang, Prestoring lithium into stable 3D nickel foam host as dendrite-free lithium metal anode, Adv. Funct. Mater. 27 (24) (2017) 1700348.
[84] Y. Li, J. Jiao, J. Bi, X. Wang, Z. Wang, L. Chen, Controlled deposition of Li metal, Nano Energy 32 (2017) 241–246.
[85] X. Zhang, A. Wang, R. Lv, J. Luo, A corrosion-resistant current collector for lithium metal anodes, Energy Storage Mater. 18 (2019) 199–204.
[86] T. Yang, et al., Lithium dendrite inhibition via 3D porous lithium metal anode accompanied by inherent SEI layer, Energy Storage Mater. 26 (2020) 385–390.
[87] P. Zou, Y. Wang, S.-W. Chiang, X. Wang, F. Kang, C. Yang, Directing lateral growth of lithium dendrites in micro-compartmented anode arrays for safe lithium metal batteries, Nat. Commun. 9 (1) (2018) 1–9.

[88] R. Zhang, et al., N-Doped graphene modified 3D porous Cu current collector toward microscale homogeneous Li deposition for Li metal anodes, Adv. Energy Mater. 8 (23) (2018) 1800914.
[89] K. Huang, Z. Li, Q. Xu, H. Liu, H. Li, Y. Wang, Lithiophilic CuO nanoflowers on Ti-mesh inducing lithium lateral plating enabling stable lithium-metal anodes with ultrahigh rates and ultralong cycle life, Adv. Energy Mater. 9 (29) (2019) 1900853.
[90] C. Zhang, et al., Vertically aligned lithiophilic CuO nanosheets on a Cu collector to stabilize lithium deposition for lithium metal batteries, Adv. Energy Mater. 8 (21) (2018) 1703404.
[91] F. Zhao, X. Zhou, W. Deng, Z. Liu, Entrapping lithium deposition in lithiophilic reservoir constructed by vertically aligned ZnO nanosheets for dendrite-free Li metal anodes, Nano Energy 62 (2019) 55–63.
[92] G. Wang, et al., Lithiated zinc oxide nanorod arrays on copper current collectors for robust Li metal anodes, Chem. Eng. J. 378 (2019) 122243.
[93] Z. Huang, et al., Realizing stable lithium deposition by in situ grown Cu 2 S nanowires inside commercial Cu foam for lithium metal anodes, J. Mater. Chem. A 7 (2) (2019) 727–732.
[94] D. Zhang, et al., Lithiophilic 3D porous CuZn current collector for stable lithium metal batteries, ACS Energy Lett. 5 (1) (2019) 180–186.
[95] S. Wu, et al., Lithiophilic Cu-CuO-Ni hybrid structure: advanced current collectors toward stable lithium metal anodes, Adv. Mater. 30 (9) (2018) 1705830.
[96] X.-Y. Yue, et al., CoO nanofiber decorated nickel foams as lithium dendrite suppressing host skeletons for high energy lithium metal batteries, Energy Storage Mater. 14 (2018) 335–344.
[97] J. Zhu, et al., Lithiophilic metallic nitrides modified nickel foam by plasma for stable lithium metal anode, Energy Storage Mater. 23 (2019) 539–546.
[98] J. Pu, et al., Conductivity and lithiophilicity gradients guide lithium deposition to mitigate short circuits, Nat. Commun. 10 (1) (2019) 1–10.
[99] Q. Li, S. Zhu, Y. Lu, 3D porous Cu current collector/Li-metal composite anode for stable lithium-metal batteries, Adv. Funct. Mater. 27 (18) (2017) 1606422.
[100] X. Chen, M. Shang, J. Niu, Inter-layer-calated thin Li metal electrode with improved battery capacity retention and dendrite suppression, Nano Lett. 20 (4) (2020) 2639–2646.
[101] L. Chen, W. Li, L.Z. Fan, C.W. Nan, Q. Zhang, Intercalated electrolyte with high transference number for dendrite-free solid-state lithium batteries, Adv. Funct. Mater. 29 (28) (2019) 1901047.
[102] S. Wu, T. Jiao, S. Yang, B. Liu, W. Zhang, K. Zhang, Lithiophilicity conversion of the Cu surface through facile thermal oxidation: boosting a stable Li–Cu composite anode through melt infusion, J. Mater. Chem. A 7 (10) (2019) 5726–5732.
[103] G. Zheng, et al., Interconnected hollow carbon nanospheres for stable lithium metal anodes, Nat. Nanotechnol. 9 (8) (2014) 618–623.
[104] Y.-j. Zhang, W.-q. Bai, X.-l. Wang, X.-h. Xia, C.-d. Gu, and J.-p. J.J. o. M.C.A. Tu, "In situ confocal microscopic observation on inhibiting the dendrite formation of a-CN x/Li electrode," vol. 4, no. 40, pp. 15597–15604, 2016.
[105] Z. Dai, et al., Engineering bifunctional host materials of sulfur and lithium-metal based on nitrogen-enriched polyacrylonitrile for Li–S batteries, Chem.–A Eur. J. (2020).
[106] T. Chen, et al., Partly lithiated graphitic carbon foam as 3D porous current collectors for dendrite-free lithium metal anodes, Electrochem. Commun. 107 (2019) 106535.
[107] W. Ye, et al., Stable nano-encapsulation of lithium through seed-free selective deposition for high-performance Li battery anodes, Adv. Energy Mater. 10 (7) (2020) 1902956.
[108] G. Yang, J. Chen, P. Xiao, P.O. Agboola, I. Shakir, Y. Xu, Graphene anchored on Cu foam as a lithiophilic 3D current collector for a stable and dendrite-free lithium metal anode, J. Mater. Chem. A 6 (21) (2018) 9899–9905.
[109] X.R. Chen, B.Q. Li, C.X. Zhao, R. Zhang, Q. Zhang, Synergetic coupling of lithiophilic sites and conductive scaffolds for dendrite-free lithium metal anodes, Small Methods 4 (6) (2020) 1900177.
[110] H. Wang, et al., Wrinkled graphene cages as hosts for high-capacity Li metal anodes shown by cryogenic electron microscopy, Nano Lett. 19 (2) (2019) 1326–1335.
[111] Y. Sun, et al., Graphite-encapsulated Li-metal hybrid anodes for high-capacity Li batteries, Chem 1 (2) (2016) 287–297.
[112] J.-S. Kim, D.W. Kim, H.T. Jung, J.W. Choi, Controlled lithium dendrite growth by a synergistic effect of multilayered graphene coating and an electrolyte additive, Chem. Mater. 27 (8) (2015) 2780–2787.
[113] H. Liu, et al., in: Mesoporous Graphene Hosts for Dendrite-Free Lithium Metal Anode in Working Rechargeable Batteries, Transactions of Tianjin University, 2020, pp. 1–8.
[114] A.-R.O. Raji, et al., Lithium batteries with nearly maximum metal storage, ACS Nano 11 (6) (2017) 6362–6369.
[115] M. Bai, et al., A scalable approach to dendrite-free lithium anodes via spontaneous reduction of spray-coated graphene oxide layers, Adv. Mater. 30 (29) (2018) 1801213.
[116] J. Qian, et al., Protecting lithium/sodium metal anode with metal-organic framework based compact and robust shield, Nano Energy 60 (2019) 866–874.
[117] X.-B. Cheng, H.-J. Peng, J.-Q. Huang, R. Zhang, C.-Z. Zhao, Q. Zhang, Dual-phase lithium metal anode containing a polysulfide-induced solid electrolyte interphase and nanostructured graphene framework for lithium–sulfur batteries, ACS Nano 9 (6) (2015) 6373–6382.
[118] H. Ye, S. Xin, Y.-X. Yin, J.-Y. Li, Y.-G. Guo, L.-J. Wan, Stable Li plating/stripping electrochemistry realized by a hybrid Li reservoir in spherical carbon granules with 3D conducting skeletons, J. Am. Chem. Soc. 139 (16) (2017) 5916–5922.
[119] Y. Chen, et al., Vertically aligned carbon nanofibers on Cu foil as a 3D current collector for reversible Li plating/stripping toward high-performance Li–S batteries, Adv. Funct. Mater. 30 (4) (2020) 1906444.
[120] F. Pei, et al., Robust lithium metal anodes realized by lithiophilic 3D porous current collectors for constructing high-energy lithium–sulfur batteries, ACS Nano 13 (7) (2019) 8337–8346.
[121] W. Liu, D. Lin, A. Pei, and Y.J.J. o. t. A. C. S. Cui, "Stabilizing lithium metal anodes by uniform Li-ion flux distribution in nanochannel confinement," vol. 138, no. 47, pp. 15443–15450, 2016.
[122] K. Shen et al., "Magnetic field–suppressed lithium dendrite growth for stable lithium-metal batteries," vol. 9, no. 20, p. 1900260, 2019.
[123] R. Zhang et al.,"Conductive nanostructured scaffolds render low local current density to inhibit lithium dendrite growth," vol. 28, no. 11, pp. 2155–2162, 2016.
[124] J. Yan, J. Yu, B. Ding, Mixed ionic and electronic conductor for Li-metal anode protection, Adv. Mater. 30 (7) (2018) 1705105.
[125] W. Guo, S. Liu, X. Guan, X. Zhang, X. Liu, J. Luo, Mixed ion and electron-conducting scaffolds for high-rate lithium metal anodes, Adv. Energy Mater. 9 (20) (2019) 1900193.
[126] Y. Zhao, et al., Carbon paper interlayers: a universal and effective approach for highly stable Li metal anodes, Nano Energy 43 (2018) 368–375.
[127] Z. Liang, et al., Polymer nanofiber-guided uniform lithium deposition for battery electrodes, Nano Lett. 15 (5) (2015) 2910–2916.
[128] Z. Wang, X. Wang, W. Sun, K. Sun, Dendrite-free lithium metal anodes in high performance lithium-sulfur batteries with bifunctional carbon nanofiber interlayers, Electrochim. Acta 252 (2017) 127–137.
[129] Y. Xu, et al., Multifunctional covalent organic frameworks for high capacity and dendrite-free lithium metal batteries, Energy Storage Mater. 25 (2020) 334–341.
[130] Y.-S. Su, A. Manthiram, Lithium–sulphur batteries with a microporous carbon paper as a bifunctional interlayer, Nat. Commun. 3 (1) (2012) 1–6.
[131] R. Singhal, S.-H. Chung, A. Manthiram, V. Kalra, A free-standing carbon nanofiber interlayer for high-performance lithium–sulfur batteries, J. Mater. Chem. A 3 (8) (2015) 4530–4538.
[132] Y. Ye, et al., A modularly-assembled interlayer to entrap polysulfides and protect lithium metal anode for high areal capacity lithium–sulfur batteries, Energy Storage Mater. 9 (2017) 126–133.
[133] H. Li, et al., Self-assembly of MoO 3-decorated carbon nanofiber interlayers for high-performance lithium–sulfur batteries, PCCP 22 (4) (2020) 2157–2163.
[134] L.-L. Kong, Z. Zhang, Y.-Z. Zhang, S. Liu, G.-R. Li, X.-P. Gao, Porous carbon paper as interlayer to stabilize the lithium anode for lithium–sulfur battery, ACS Appl. Mater. Interfaces 8 (46) (2016) 31684–31694.
[135] Z. Sun, Y. Guo, B. Li, T. Tan, Y. Zhao, ZnO/carbon nanotube/reduced graphene oxide composite film as an effective interlayer for lithium/sulfur batteries, Solid State Sci. 95 (2019) 105924.
[136] C. Li, et al., Two-dimensional molecular brush-functionalized porous bilayer composite separators toward ultrastable high-current density lithium metal anodes, Nat. Commun. 10 (1) (2019) 1–9.
[137] C. Niu, et al., Self-smoothing anode for achieving high-energy lithium metal batteries under realistic conditions, Nat. Nanotechnol. 14 (6) (2019) 594–601.
[138] K. Yan, et al., Selective deposition and stable encapsulation of lithium through heterogeneous seeded growth, Nat. Energy 1 (3) (2016) 1–8.
[139] Z. Liang, et al., Composite lithium metal anode by melt infusion of lithium into a 3D conducting scaffold with lithiophilic coating, Proc. Natl. Acad. Sci. 113 (11) (2016) 2862–2867.
[140] G. Hou, et al., Dendrite-free Li metal anode enabled by a 3D free-standing lithiophilic nitrogen-enriched carbon sponge, J. Power Sources 386 (2018) 77–84.
[141] Z. Zhao, et al., N-doped porous carbon-graphene cables synthesized for self-standing cathode and anode hosts of Li–S batteries, Electrochim. Acta (2020) 136231.
[142] Z. Lyu, et al., 3D-printed electrodes for lithium metal batteries with high areal capacity and high-rate capability, Energy Storage Mater. 24 (2020) 336–342.
[143] T. Jiang, et al., Nitrogen-doped graphdiyne nanowall stabilized dendrite-free lithium metal anodes, J. Mater. Chem. A 7 (48) (2019) 27535–27546.
[144] L. Liu, Y.X. Yin, J.Y. Li, S.H. Wang, Y.G. Guo, L.J. Wan, Uniform lithium nucleation/growth induced by lightweight nitrogen-doped graphitic carbon foams for high-performance lithium metal anodes, Adv. Mater. 30 (10) (2018) 1706216.
[145] P. Zhai, et al., Uniform lithium deposition assisted by single-atom doping toward high-performance lithium metal anodes, Adv. Energy Mater. 9 (18) (2019) 1804019.
[146] R. Zhang, et al., Lithiophilic sites in doped graphene guide uniform lithium nucleation for dendrite-free lithium metal anodes, Angew. Chem. 129 (27) (2017) 7872–7876.
[147] X. Chen, et al., Lithiophilicity chemistry of heteroatom-doped carbon to guide uniform lithium nucleation in lithium metal anodes, Sci. Adv. 5 (2) (2019) eaau7728.
[148] C. Jin, et al., 3D lithium metal embedded within lithiophilic porous matrix for stable lithium metal batteries, Nano Energy 37 (2017) 177–186.
[149] H. Zhang, et al., Lithiophilic-lithiophobic gradient interfacial layer for a highly stable lithium metal anode, Nat. Commun. 9 (1) (2018) 1–11.
[150] L. Tang, et al., ZnO nanoconfined 3D porous carbon composite microspheres to stabilize lithium nucleation/growth for high-performance lithium metal anodes, J. Mater. Chem. A 7 (33) (2019) 19442–19452.
[151] W. Deng, W. Zhu, X. Zhou, Z. Liu, Graphene nested porous carbon current collector for lithium metal anode with ultrahigh areal capacity, Energy Storage Mater. 15 (2018) 266–273.
[152] L. Wang, et al., ZnO/carbon framework derived from metal-organic frameworks as a stable host for lithium metal anodes, Energy Storage Mater. 11 (2018) 191–196.
[153] T.-T. Zuo, et al., Trapping lithium into hollow silica microspheres with a carbon nanotube core for dendrite-free lithium metal anodes, Nano Lett. 18 (1) (2018) 297–301.

[154] X. Ji, D.-Y. Liu, D.G. Prendiville, Y. Zhang, X. Liu, G.D. Stucky, Spatially heterogeneous carbon-fiber papers as surface dendrite-free current collectors for lithium deposition, Nano Today 7 (1) (2012) 10–20.
[155] B. Yu, T. Tao, S. Mateti, S. Lu, Y. Chen, Nanoflake arrays of lithiophilic metal oxides for the ultra-stable anodes of lithium-metal batteries, Adv. Funct. Mater. 28 (36) (2018) 1803023.
[156] K. Lin, et al., Ultrafine titanium nitride sheath decorated carbon nanofiber network enabling stable lithium metal anodes, Adv. Funct. Mater. 29 (46) (2019) 1903229.
[157] Z. Guo, et al., Lithiophilic Co/Co 4 N nanoparticles embedded in hollow N-doped carbon nanocubes stabilizing lithium metal anodes for Li–air batteries, J. Mater. Chem. A 6 (44) (2018) 22096–22105.
[158] P. Shi, et al., Lithiophilic LiC6 layers on carbon hosts enabling stable Li metal anode in working batteries, Adv. Mater. 31 (8) (2019) 1807131.
[159] S. Liu, et al., 3D TiC/C core/shell nanowire skeleton for dendrite-free and long-life lithium metal anode, Adv. Energy Mater. 8 (8) (2018) 1702322.
[160] X. Tang, X. Guo, W. Wu, G. Wang, 2D metal carbides and nitrides (MXenes) as high-performance electrode materials for lithium-based batteries, Adv. Energy Mater. 8 (33) (2018) 1801897.
[161] G. Jiang, et al., MOF-derived porous Co3O4-NC nanoflake arrays on carbon fiber cloth as stable hosts for dendrite-free Li metal anodes, Energy Storage Mater. 23 (2019) 181–189.
[162] M. Zhu, B. Li, S. Li, Z. Du, Y. Gong, S. Yang, Dendrite-free metallic lithium in lithiophilic carbonized metal–organic frameworks, Adv. Energy Mater. 8 (18) (2018) 1703505.
[163] L. Chen, et al., Self-supporting lithiophilic N-doped carbon rod array for dendrite-free lithium metal anode, Chem. Eng. J. 363 (2019) 270–277.
[164] G. Huang, et al., Lithiophilic 3D nanoporous nitrogen-doped graphene for dendrite-free and ultrahigh-rate lithium-metal anodes, Adv. Mater. 31 (2) (2019) 1805334.
[165] X. Zhang et al., "Vertically aligned and continuous nanoscale ceramic–polymer interfaces in composite solid polymer electrolytes for enhanced ionic conductivity," vol. 18, no. 6, pp. 3829–3838, 2018.
[166] J. Cui, S. Yao, M. Ihsan-Ul-Haq, J. Wu, J.K. Kim, Correlation between Li plating behavior and surface characteristics of carbon matrix toward stable Li metal anodes, Adv. Energy Mater. 9 (1) (2019) 1802777.
[167] L. Tao, et al., A surface chemistry approach to tailoring the hydrophilicity and lithiophilicity of carbon films for hosting high-performance lithium metal anodes, Adv. Funct. Mater. (2020) 2000585.
[168] Y. Liu, et al., Oxygen and nitrogen co-doped porous carbon granules enabling dendrite-free lithium metal anode, Energy Storage Mater. 18 (2019) 320–327.
[169] C. Ma, C. Deng, X. Liao, Y. He, Z. Ma, H. Xiong, Nitrogen and phosphorus codoped porous carbon framework as anode material for high rate lithium-ion batteries, ACS Appl. Mater. Interfaces 10 (43) (2018) 36969–36975.
[170] J. Pu, et al., Interlayer lithium plating in Au nanoparticles pillared reduced graphene oxide for lithium metal anodes, Adv. Funct. Mater. 28 (41) (2018) 1804133.
[171] Y. Yang, J. Xiong, J. Zeng, J. Huang, J. Zhao, VGCF 3D conducting host coating on glass fiber filters for lithium metal anodes, Chem. Commun. 54 (10) (2018) 1178–1181.
[172] C. Yang, Y. Yao, S. He, H. Xie, E. Hitz, L. Hu, Ultrafine silver nanoparticles for seeded lithium deposition toward stable lithium metal anode, Adv. Mater. 29 (38) (2017) 1702714.
[173] R. Zhang, et al., Coralloid carbon fiber-based composite lithium anode for robust lithium metal batteries, Joule 2 (4) (2018) 764–777.
[174] Y. Sun, J. Zhou, H. Ji, J. Liu, T. Qian, C. Yan, Single-atom iron as lithiophilic site to minimize lithium nucleation overpotential for stable lithium metal full battery, ACS Appl. Mater. Interfaces 11 (35) (2019) 32008–32014.
[175] G. Xiao, et al., N-doped carbon nanotubes decorated with Fe/Ni sites to stabilize lithium metal anodes, Inorg. Chem. Front. (2020).
[176] S.W. Lee, et al., High-power lithium batteries from functionalized carbon-nanotube electrodes, Nat. Nanotechnol. 5 (7) (2010) 531–537.
[177] H. Liu, et al., Lithium metal anodes: uniform lithium nucleation guided by atomically dispersed lithiophilic CoNx sites for safe lithium metal batteries (small methods 9/2019), Small Methods 3 (9) (2019) 1970026.
[178] S. Li, et al., Hierarchical Co3O4 nanofiber–carbon sheet skeleton with superior Na/Li-philic property enabling highly stable alkali metal batteries, Adv. Funct. Mater. 29 (19) (2019) 1808847.
[179] T.S. Wang, X. Liu, X. Zhao, P. He, C.W. Nan, L.Z. Fan, Regulating uniform Li plating/stripping via dual-conductive metal-organic frameworks for high-rate lithium metal batteries, Adv. Funct. Mater. 30 (16) (2020) 2000786.
[180] S. Liu, et al., Superhierarchical cobalt-embedded nitrogen-doped porous carbon nanosheets as two-in-one hosts for high-performance lithium–sulfur batteries, Adv. Mater. 30 (12) (2018) 1706895.
[181] J. Li, D. Yan, S. Hou, T. Lu, Y. Yao, L. Pan, Metal-organic frameworks converted flower-like hybrid with Co3O4 nanoparticles decorated on nitrogen-doped carbon sheets for boosted lithium storage performance, Chem. Eng. J. 354 (2018) 172–181.
[182] J. Lee, et al., Structurally stabilized lithium-metal anode via surface chemistry engineering, Energy Storage Mater. 37 (2021) 315–324.
[183] X. Li, et al., Redistributing Li-ion flux and homogenizing Li-metal growth by N–doped hierarchically porous membranes for dendrite-free Lithium metal batteries, Energy Storage Mater. 37 (2021) 233–242.
[184] Y. Zhao, W. Wu, J. Li, Z. Xu, L. Guan, Encapsulating MWNTs into hollow porous carbon nanotubes: a tube-in-tube carbon nanostructure for high-performance lithium-sulfur batteries, Adv. Mater. 26 (30) (2014) 5113–5118.
[185] J.R. Sanchez-Valencia, et al., Controlled synthesis of single-chirality carbon nanotubes, Nature 512 (7512) (2014) 61–64.
[186] Y.-X. Zhan, et al., The insights of lithium metal plating/stripping in porous hosts: progress and perspectives, Energy Technol. 9 (2) (2021) 2000700.
[187] Y. Zhong, et al., Popcorn inspired porous macrocellular carbon: rapid puffing fabrication from rice and its applications in lithium–sulfur batteries, Adv. Energy Mater. 8 (1) (2018) 1701110.
[188] S. Feng, et al., Assembling carbon pores into carbon sheets: rational design of three-dimensional carbon networks for a lithium–sulfur battery, ACS Appl. Mater. Interfaces 11 (6) (2019) 5911–5918.
[189] H.J. Peng, et al., Strongly coupled interfaces between a heterogeneous carbon host and a sulfur-containing guest for highly stable lithium-sulfur batteries: mechanistic insight into capacity degradation, Adv. Mater. Interfaces 1 (7) (2014) 1400227.
[190] P.-Y. Zhai, et al., Scaled-up fabrication of porous-graphene-modified separators for high-capacity lithium–sulfur batteries, Energy Storage Mater. 7 (2017) 56–63.
[191] M.-Q. Zhao, et al., Unstacked double-layer templated graphene for high-rate lithium–sulphur batteries, Nat. Commun. 5 (1) (2014) 1–8.
[192] H. Geng, Y. Peng, L. Qu, H. Zhang, M. Wu, Structure design and composition engineering of carbon-based nanomaterials for lithium energy storage, Adv. Energy Mater. 10 (10) (2020) 1903030.
[193] Y. Zhang, et al., High-capacity, low-tortuosity, and channel-guided lithium metal anode, Proc. Natl. Acad. Sci. 114 (14) (2017) 3584–3589.
[194] X.-Y. Yue, et al., Copper decorated ultralight 3D carbon skeleton derived from soybean oil for dendrite-free Li metal anode, Chem. Eng. J. (2019) 123516.
[195] J. Lang, et al., Surface graphited carbon scaffold enables simple and scalable fabrication of 3D composite lithium metal anode, J. Mater. Chem. A 5 (36) (2017) 19168–19174.
[196] W. Go, et al., Nanocrevasse-rich carbon fibers for stable lithium and sodium metal anodes, Nano Lett. 19 (3) (2018) 1504–1511.
[197] X. Wang, et al., Infiltrating lithium into carbon cloth decorated with zinc oxide arrays for dendrite-free lithium metal anode, Nano Res. 12 (3) (2019) 525–529.
[198] M.S. Kim, et al., Langmuir–Blodgett artificial solid-electrolyte interphases for practical lithium metal batteries, Nat. Energy 3 (10) (2018) 889–898.
[199] J. Xie, et al., Incorporating flexibility into stiffness: self-grown carbon nanotubes in melamine sponges enable a lithium-metal-anode capacity of 15 mA h cm− 2 cyclable at 15 mA cm− 2, Adv. Mater. 31 (7) (2019) 1805654.
[200] C. Zhao, et al., Implanting CNT forest onto carbon nanosheets as multifunctional hosts for high-performance lithium metal batteries, Small Methods 3 (5) (2019) 1800546.
[201] R. Mukherjee, et al., Defect-induced plating of lithium metal within porous graphene networks, Nat. Commun. 5 (1) (2014) 1–10.
[202] S. Matsuda, Y. Kubo, K. Uosaki, S. Nakanishi, Lithium-metal deposition/dissolution within internal space of CNT 3D matrix results in prolonged cycle of lithium-metal negative electrode, Carbon 119 (2017) 119–123.
[203] Y. Zhang, et al., A 3D lithium/carbon fiber anode with sustained electrolyte contact for solid-state batteries, Adv. Energy Mater. 10 (3) (2020) 1903325.
[204] B. Li, D. Zhang, Y. Liu, Y. Yu, S. Li, S. Yang, Flexible Ti3C2 MXene-lithium film with lamellar structure for ultrastable metallic lithium anodes, Nano Energy 39 (2017) 654–661.
[205] X. Shen, et al., Lithium–matrix composite anode protected by a solid electrolyte layer for stable lithium metal batteries, J. Energy Chem. 37 (2019) 29–34.
[206] D. Lin, et al., A high tap density secondary silicon particle anode fabricated by scalable mechanical pressing for lithium-ion batteries, Energy Environ. Sci. 8 (8) (2015) 2371–2376.
[207] F. Guo, et al., Advanced lithium metal–carbon nanotube composite anode for high-performance lithium–oxygen batteries, Nano Lett. 19 (9) (2019) 6377–6384.
[208] T. Li, H. Liu, P. Shi, Q. Zhang, Recent progress in carbon/lithium metal composite anode for safe lithium metal batteries, Rare Met. 37 (6) (2018) 449–458.
[209] P. Shi, X.Q. Zhang, X. Shen, R. Zhang, H. Liu, Q. Zhang, A review of composite lithium metal anode for practical applications, Adv. Mater. Technol. 5 (1) (2020) 1900806.
[210] N. Shu, et al., Rolling press of lithium with carbon for high-performance anodes, Energy Storage Mater. 24 (2020) 689–693.
[211] X. Zhou, et al., Enabling lithium-metal anode encapsulated in a 3D carbon skeleton with a superior rate performance and capacity retention in full cells, ACS Appl. Mater. Interfaces 10 (41) (2018) 35296–35305.
[212] F. Liu, et al., Regulating lithium nucleation via CNTs modifying carbon cloth film for stable Li metal anode, Small 15 (5) (2019) 1803734.
[213] Y. Zhang, et al., A carbon-based 3D current collector with surface protection for Li metal anode, Nano Res. 10 (4) (2017) 1356–1365.
[214] G. Yang et al., "Iron carbide allured lithium metal storage in carbon nanotube cavities," vol. 36, pp. 459–465, 2021.
[215] Y.-S. Hong, N. Li, H. Chen, P. Wang, W.-L. Song, and D.J.E.S.M. Fang, "In operando observation of chemical and mechanical stability of Li and Na dendrites under quasi-zero electrochemical field," vol. 11, pp. 118–126, 2018.
[216] J. Lee et al., "Structurally stabilized lithium-metal anode via surface chemistry engineering," vol. 37, pp. 315–324, 2021.
[217] R. Zhang et al., "Atomic layer deposition assisted superassembly of ultrathin ZnO layer decorated hierarchical Cu foam for stable lithium metal anode," vol. 37, pp. 123–134, 2021.
[218] E. Peled, The electrochemical behavior of alkali and alkaline earth metals in nonaqueous battery systems—the solid electrolyte interphase model, J. Electrochem. Soc. 126 (12) (1979) 2047.
[219] K. Kanamura, S. Shiraishi, Z.i. Takehara, Electrochemical deposition of very smooth lithium using nonaqueous electrolytes containing HF, J. Electrochem. Soc. 143 (7) (1996) 2187.

[220] Y. Ein-Eli, A new perspective on the formation and structure of the solid electrolyte interface at the graphite anode of Li-ion cells, Electrochem. Solid State Lett. 2 (5) (1999) 212.
[221] L. Li, Self-heating–induced healing of lithium dendrites, Science 359 (6383) (2018) 1513–1516.
[222] D. Cao, 3D printed high-performance lithium metal microbatteries enabled by nanocellulose, Adv. Mater. 31 (14) (2019) 1807313.
[223] R. Zhang, X. Shen, X.-B. Cheng, Q. Zhang, The dendrite growth in 3D structured lithium metal anodes: electron or ion transfer limitation? Energy Storage Mater. 23 (2019) 556–565.
[224] J. Thevenin, R. Muller, Impedance of lithium electrodes in a propylene carbonate electrolyte, J. Electrochem. Soc. 134 (2) (1987) 273.
[225] J. Thevenin, Passivating films on lithium electrodes. An approach by means of electrode impedance spectroscopy, J. Power Sources 14 (1-3) (1985) 45–52.
[226] F. Han, et al., High electronic conductivity as the origin of lithium dendrite formation within solid electrolytes, Nat. Energy 4 (3) (2019) 187–196.
[227] D.H. Tan, A. Banerjee, Z. Chen, Y.S. Meng, From nanoscale interface characterization to sustainable energy storage using all-solid-state batteries, Nat. Nanotechnol. (2020) 1–11.
[228] A. Manthiram, X. Yu, S. Wang, Lithium battery chemistries enabled by solid-state electrolytes, Nat. Rev. Mater. 2 (4) (2017) 1–16.
[229] Y. Xiao, Y. Wang, S.-H. Bo, J.C. Kim, L.J. Miara, G. Ceder, Understanding interface stability in solid-state batteries, Nat. Rev. Mater. (2019) 1–22.
[230] Y.-G. Lee, et al., High-energy long-cycling all-solid-state lithium metal batteries enabled by silver–carbon composite anodes, Nat. Energy 5 (4) (2020) 299–308.